New Journal and we have not received input yet 21 (2021) 100791

Contents lists available at ScienceDirect

Thermal Science and Engineering Progress

journal homepage: www.sciencedirect.com/journal/thermal-science-and-engineering-progress

Experimental investigation into the integration of solid desiccant packed beds with oscillating heat pipes for energy efficient isothermal adsorption processes

S.K. Yeboah [a,*], J. Darkwa [b]

[a] Department of Architecture and Built Environment, Faculty of Science and Engineering, The University of Nottingham Ningbo China, 199 Taikang East Road, Ningbo 315100, PR China

[b] Department of Architecture and Built Environment, The University of Nottingham, University Park, Nottingham NG7 2RD, UK

ARTICLE INFO

Keywords:
Heat of adsorption
Packed beds
Heat and mass transfer
Oscillating heat pipes
Thermal management
Thermal performance

ABSTRACT

The heat of adsorption released during physical adsorption of water vapour on solid desiccants increases its surface vapour pressure consequently decreasing its adsorption capacity. In packed beds, this raises the bed temperature subsequently increasing the cooling load and energy required for the regeneration of the solid desiccants. In this study, we experimentally investigated helically coiled oscillating heat pipes (HCOHPs) using ethanol, methanol and deionized water respectively as working fluids integrated with packed beds of varying configurations towards isothermal adsorption. The results show average bed temperature reduction varied with heat output from the bed and the thermal performance of the HCOHPs. The fully packed bed (FPB) integrated with the ethanol HCOHP (EOHP) achieved maximum average bed temperature reduction of 14.0 °C. The annulus packed bed (APB) integrated with the water HCOHP (WOHP) achieved a temperature drop of 10.1 °C. Adsorption peak temperature reductions on the other hand were strongly dependent on HCOHP start-up. Maximum adsorption peak temperature reduction of 20.8 °C in Mass Transfer Zone (MTZ) 1 was attained by the FPB-EOHP integrated system. For the APB, maximum adsorption peak temperature reduction of 13.2 °C in MTZ 3 was recorded for Small APB (SAPB)-Methanol HCOHP (MOHP) integrated system. Adsorption rates in the FPB were influenced by the mal-distribution of flow within the bed and increased slightly on integration with the HCOHPs. Maximum adsorption rates of 1.47×10^{-06} kg/s was achieved by the FPB-EOHP. For the APB, the SAPB-WOHP achieved maximum adsorption rates of 1.21×10^{-05}kg/s. The adsorption rates in the Medium APB (MAPB) on the other hand did not appear to be influenced on integration with the HCOHPs. Overall, performances of the integrated systems were found to be influenced partly by the packed bed configuration, the HCOHPs' performance and the heat transfer resistance between the evaporators and the vessel walls. We recommend further optimization of the system parameters and investigation of its regeneration potential for future practical applications.

1. Introduction

Effective dehumidification can be achieved when process air is passed through nano-porous solids such as silica gel for water vapour adsorption [1–3]. However, the spontaneous and exothermic nature of the physical adsorption process generates the isosteric heat of adsorption equal to the latent heat of evaporation and an additional amount of heat due to a change in the surface energy of the solid desiccant [4–7]. In a packed bed of solid desiccants, this heat raises the temperature of the bed and decreases the adsorption capacity, subsequently changing the exit process airstream humidity ratio [8,9]. Abd-Elrahman et al. [1] found that the adsorption heat raises the vapour pressure on the bed surface subsequently decreasing the mass transfer potential. Ramzy et al. [2] also observed the exothermic adsorption process increases the bed temperature and decreases the sorption capacity of the solid desiccants. Do [10] asserts that the isosteric heat of adsorption slows down the adsorption kinetics because the mass uptake is controlled by the rate of cooling of the particle in the later course of adsorption. Yeboah and Darkwa [11] found that the heat of adsorption released during the adsorption of water vapour in a packed bed of adsorbent particles significantly reduces adsorption capacity which impinges on the energy

* Corresponding author.
E-mail addresses: Siegfried.yeboah@nottingham.edu.cn (S.K. Yeboah), J.Darkwa@nottingham.ac.uk (J. Darkwa).

https://doi.org/10.1016/j.tsep.2020.100791
Received 6 August 2020; Received in revised form 12 November 2020; Accepted 17 November 2020
Available online 28 November 2020

Nomenclature

A	cross sectional area, m2
C_{pg}	specific heat of silica gel (kJ/kg)
cp_s	specific heat of air at constant pressure (kJ/kg K)
cp_w	specific heat of water content in the bed (kJ/kg K)
f_s	dimensionless enhancement factor
h	enthalpy
k	material thermal conductivity (W/m·K)
L	length (m)
p	ambient pressure (kPa)
p_v	water vapour pressure (kPa)
p_g	saturated water vapour pressure (kPa)
RH	relative humidity (%)
Q	heating power input (W)
q_{av}	the average heat flux of the vessel and evaporator coils (W/m2)
Q_v	volume flow rate (m3/s)
q_v	heat flux from the vessel (W/m2)
q_{evap}	heat flux at the evaporator (W/m2)
R	thermal resistance (°C/W)
r_i	inner radius of packed bed vessel (m)
r_o	outer radius of packed bed vessel (m)
t	time (s)
T	Temperature (K or °C)
ΔT	temperature difference (K)
T_{evap}	the surface temperatures of evaporator coils at the contact interface (°C)
T_{gi}	air temperature at the bed inlet (K)
T_i	inner surface temperature of packed bed vessel (K)
T_o	outer surface temperature of packed bed vessel (K)
T_v	the surface temperatures of vessel at the contact interface (°C)
T_p	bed temperature (K)
u_o	superficial air velocity flowing in the bed (m/s)
W	water content of silica gel (kg/kg)

Greek Letters

ε	void fraction of silica gel particle
ρ_g	air density (kg/m3)
ρ_s	dry silica gel density (kg/m3)
ω_{in} and ω_{out}	inlet and outlet humidity ratios (kg/kg)
ω i	humidity ratio/moisture content (kg/kg)
ω_s	saturated moisture content (kg/kg)
θ	temperature, greater than or equal to 0 °C.

Abbreviations

EOHP	Ethanol Oscillating Heat Pipe
FPB	Fully Packed Bed
HCOHP	Helically Coiled Oscillating Heat Pipe
APB	Annulus Packed Bed
LAPB	Large Annulus Packed Bed
MAPB	Medium Annulus Packed Bed
MOHP	Methanol Oscillating Heat Pipe
MTZ	Mass Transfer Zone
SAPB	Small Annulus Packed Bed
TC	Thermocouple
TR	Thermal Resistance
WOHP	Water Oscillating Heat Pipe

efficiency of any solid desiccant dehumidification system. Nobrega and Brum [12] found isothermal adsorptive process theoretically accomplished by using an infinite number of desiccant stages intercalated with infinite intercoolers more effective than the adiabatic adsorptive process. According to Pistocchini et al. [13], adsorption heat removal causes a decrease in dehumidified air temperature, by allowing sensibly higher relative humidity for outlet air, so that the regeneration phase can be performed at higher levels of relative humidity. This keeps the driving force of the cycle average difference of relative humidity between dehumidification and regeneration phase at the same value compared to the adiabatic process. In their study, they found that this accounts for a significant reduction of air temperature required by the regeneration phase (51 °C), compared to 70 °C when following the adiabatic process.

For solid desiccant packed beds, the amount of adsorbable species adsorbed depends on the temperature at the solid desiccant surface hence managing in situ the heat transfer within the bed is found to enhance the efficiency of the sorption process [13,14]. For instance, packed beds have been designed with small tube to particle diameter ratios to dissipate heat via their walls however investigations by Kwapinski et al. [14] shows that this results in the mal-distribution of flow near the walls which impacts on fluid residence time in the bed. Others [15–22] have investigated the use of internal cooling coils to remove heat from adsorbent beds for isothermal adsorption. Clausse et al. [17] studied the behaviour differences between an indirectly cooled Temperature Swing Adsorption (TSA) packed bed adsorber and other classical adsorbers such as adiabatic, near-adiabatic and isothermal packed bed systems. They observed that for the adiabatic adsorber, a high initial bed temperature strongly reduces the performance. Also, their new TSA adsorber can minimize the initial bed temperature due to the heat exchanger's capability to cool the whole column simultaneously. Bonjour et al. [18] investigated the performance of a TSA packed bed adsorber with an internal heat-exchanger and found the adsorption cycle performance increased when the regeneration temperature increased, representing an increase in energy consumption compared to conventional systems. Pirngruber et al. [19] installed a heat exchanger in a TSA adsorber to operate it isothermally and found that an increase in the heat exchanger size results in better heat transfer although it increases the thermal inertia of the bed. Niazmand and Dabzadeh [20] found that placing annular fins in a silica gel packed bed adsorber reduces the COP of the cooling cycle however simultaneous desorption and adsorption processes can also occur in different sections of the bed depending on their locations and transient histories. Sircar [21] used forced convection for the removal of the heat of adsorption and found that even a fairly high gas flow rate over the adsorbent may not be sufficient to produce isothermal uptake, particularly when the adsorbate mass transfer coefficient is moderately large. Rady et al. [8], and Meljac et al. [14] integrated inert particles such as phase change materials (PCMs) to act as heat sinks. Meljac et al. [14] observed that without a thermal binder hot spots were generated in the bed whilst Rady et al. [8] found that the sudden increase of bed temperature at the beginning was absent since the heat generated from the adsorption of water vapour was used to melt the encapsulated PCM. They observed the bed temperature remained constant until all the PCM melted and then it started to increase with time to reach a peak value before decreasing. They also encountered challenges in adopting the PCM latent heat, melting temperature and quantity to the process parameters. Hung et al. [22] investigated the thermal performances of solid desiccant tray having internal cooling/heating coil for air humidity adsorption and desiccant regeneration and found their technique could enhance the performance of both adsorption and regeneration processes. Investigations by Mulgundmath et al. [23] also shows that cooling during the adsorption cycle decreases the width of the mass transfer zone and leads to longer breakthrough times.

Oscillating heat pipes offer enhanced heat transfer through passive

two-phase heat transfer mechanism [24,25]. Developed by Akachi [26] in 1990, they are widely applied to achieve thermal management solutions in systems. For instance, Qu et al. [27] evaluated the effects of adiabatic length and structural style of three flexible oscillating heat pipes (FOHPs) on start-up, evaporator temperature and overall thermal resistance and found that they can provide thermal management solutions for electric/hybrid-electric vehicle battery. Wei et al. [28] developed a proof-of-concept plug-in oscillating heat pipe (OHP) with flat-plate evaporator and tube condenser. They experimentally tested its potential application in EV battery thermal management and found that the average battery pack temperature could be controlled below 46.5 °C under the power input of 56 W. Qu et al. [29] experimentally investigated the enhancement of phase change materials (PCM) using oscillating heat pipe (OHP) and found that the OHP can help the system reach thermal equilibrium stage during the thermal management process after start-up. Qian et al. [30] on the other hand proposed a novel heat transfer prediction model of oscillating heat pipes based on the extreme gradient boosting algorithm (XGBoost) to choose suitable geometry and cooling methods of OHPs for enhancing heat transfer in machining processes. They found their model provides a reliable foundation for the application of OHPs in machining processes for augmented heat transfer. Wang et al. [31] developed a novel tubular oscillating heat pipe (OHP) with sintered copper particles (SCPs) inside a flat-plate evaporator for the thermal management of high-power LED chips and achieved a lower thermal resistance of 0.168 K/W by the OHP with SCPs when the input power to the LED array was 60 W. They also found that the corresponding maximum LED temperature can be controlled below 70 °C.

In our previous work [32], we developed helically coiled oscillating heat pipes (HCOHPs) charged with ethanol, methanol and deionized water respectively at approximately 60% volume fill ratio and tested them under laboratory conditions to evaluate their capacity to cool adsorption packed beds. In subsequent studies [33], we experimentally investigated the influence of the Heggs et al. [34] Z-annulus configuration on the enhancement of the physical adsorption process. The study also builds up on work done by Yeboah [35]. In this present investigation, we have integrated the HCOHPs that we developed [32] with the investigated [33] solid desiccant packed bed adsorbers in order to evaluate their thermal effectiveness for isothermal adsorption processes. As passive two-phase heat transfer devices [24,25], the Helically Coiled Oscillating Heat Pipes (HCOHPs) do not require external energy for the cooling of the solid desiccant packed bed adsorbers and the whole process is envisaged to help achieve an isothermal adsorption process.

2. Experimental setup and procedure

2.1. Description of physical model

The experimental set up had three similar helically coiled single closed loop oscillating heat pipes (HCOHPs) integrated with a packed bed adsorber for isothermal adsorption (See Fig. 1). For each set up, three HCOHPs containing same working fluid at similar fill ratios oriented vertically were integrated at three designated mass transfer zones (MTZ) on the packed bed vessel.

The theoretical concept of the integrated packed bed-HCOHP system is that the packed bed undergoes adsorption whilst the evaporators of the HCOHPs passively remove the heat of adsorption released via the walls of the vessel. The evaporators transfer the heat generated in the bed to the condenser which is then rejected to the ambient surroundings via natural convection. With this process, the HCOHPs passively cool the adsorbing bed with the aim of reducing the bed temperature to achieve isothermal adsorption process.

2.2. Experimental methodology

The packed bed and its varied Z-annulus configurations were integrated respectively with three HCOHPs having the same working fluid for each experimental run. Three sets of HCOHPs were each filled with ethanol, methanol and deionised water as working fluids as shown in Fig. 2a. These three working fluids were chosen as they operated within the peak adsorption temperatures of the packed beds as established by Yeboah and Darkwa [33]. This was considered along with their compatibility with the heat pipe material of copper, their thermophysical properties and the figure of merit as determined in the study by Yeboah and Darkwa [36].

The packed beds were designated Fully Packed Bed (FPB), Large Annulus Packed Bed (LAPB), Medium Annulus Packed Bed (MAPB) and Small Annulus Packed Bed (SAPB) as per our previous study [33]. The annulus structures (See Fig. 2b) were determined within the ranges obtained from literature [15,34,37] and the designations represented outer and inner diameter ratios(D_o/D_i) of 2, 2.35 and 3.08 corresponding to LAPB, MAPB and SAPB, respectively. The main copper vessel itself was 30 cm long with an outer diameter of 8 cm (See Figs. 2c and 2d). The packed bed was first tested empty and then with packed silica gel particles (size ranging between 3.35 and 4.75 mm) in order to determine the respective outlet bed velocities. The mixing box incorporated a 300 W fan heater that provided a maximum inlet air velocity of 2.48 m/s for the tests. The maximum inlet air velocity was used because during the testing it was found that there was significant pressure drops due to the internal configuration of the beds leading to lower outlet velocities. For the empty vessel, an average outlet velocity of 1.81 m/s was recorded at the maximum inlet velocity. While average outlet velocities of 0.45 m/s, 0.52 m/s and 0.45 m/s were recorded respectively for the LAPB, MAPB and SAPB when densely packed with silica gel particles and the inlet velocity was kept at the maximum. Varying the fan speed to lower inlet velocities although minimized energy consumption of the air heater resulted in significantly lower outlet velocities difficult for the velocity to be measured by the Sentry ST732 Hotwire Anemometer. Even at this maximum inlet velocity, the FPB had a significantly lower outlet velocity averaging about 0.03 m/s due to the dense random nature of the silica gel packing indicating significant pressure drop with this packed bed configuration. With the packing (bulk) density and the particle density determined, a bed porosity of 0.44 was obtained. K-type thermocouples (TCs) were inserted in the three mass transfer zones, MTZ 1, MTZ 2 and MTZ 3, and on corresponding walls of the packed bed. The filling of the packed beds was done carefully to ensure that the interior thermocouple positions were not altered to influence measurements. For the annulus packed beds, thermocouples were placed between the walls and the annulus mesh pipe via each designated mass transfer zone (See Fig. 2d). For the fully packed bed, the interior thermocouples were inserted to approximately the middle of each cross section of the designated mass transfer zones of the bed.

For the HCOHPs, the ethanol (C_2H_5OH) fluid type is presented as EOHP, the methanol(CH_3OH) as MOHP and the deionised water (H_2O)as WOHP [32]. The HCOHPs were made of copper tubes of internal diameter, 2 mm and thickness, 1 mm. Each evaporator and condenser coil were of 10 turns respectively with a coil diameter of 8 cm. The designated adiabatic section was 20 cm long. The HCOHPs were evacuated to a pressure of about 0.0013 MPa before being charged with the respective working fluids to a volume ratio of 60%.

The integration was done such that the evaporator coils of the HCOHPs were in direct contact with the walls of the packed bed vessel and each HCOHP covered one of the designated mass transfer zones. Thermocouples were also attached to the respective evaporator, condenser, and adiabatic sections of the integrated HCOHPs and connected to the Yokogawa MV2000 and the desktop computer as shown in the schematic in Fig. 3a. For each HCOHP, the first, middle and last rings of the evaporator and condenser coils were connected to a thermocouple, respectively. The packed bed system attached to the evaporator sections of the HCOHPs were then insulated with a 20 mm thick nitrile rubber thermal insulation material as shown in Fig. 3b.

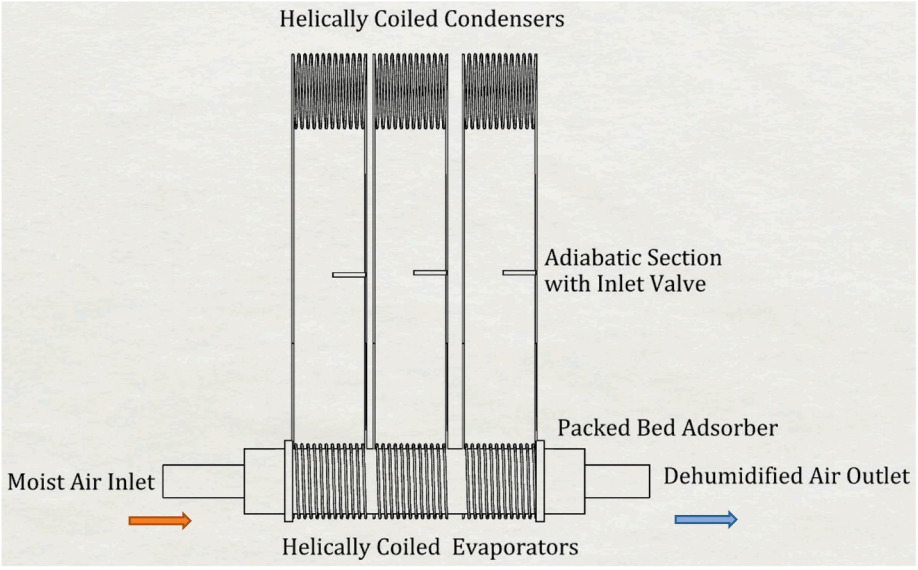

Fig. 1. Schematic of the three Helically Coiled Oscillating Heat Pipes (HCOHPs) Integrated with the Packed Bed

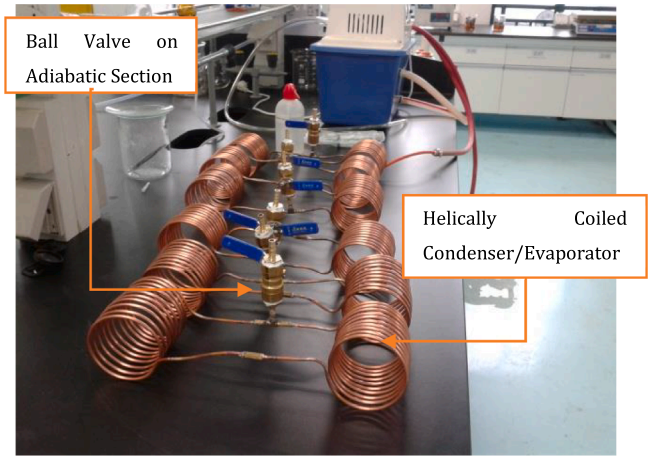

Fig. 2a. HCOHPs Charged with Working Fluids in the Laboratory

Fig. 2c. Cross-section of the Insulated Packed Bed Vessel Filled with Silica Gel

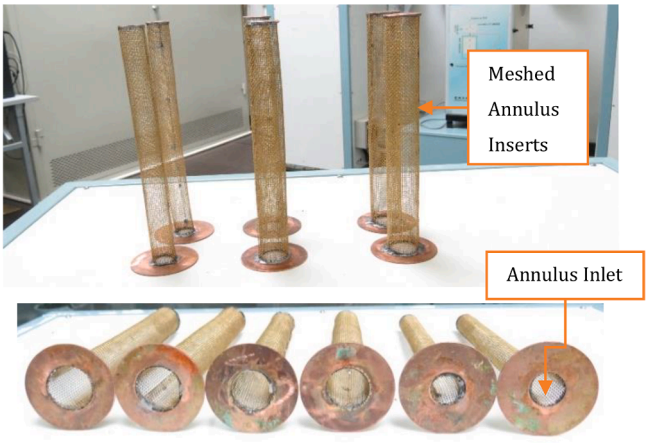

Fig. 2b. Meshed Annulus Inserts with Varying Inner Diameters

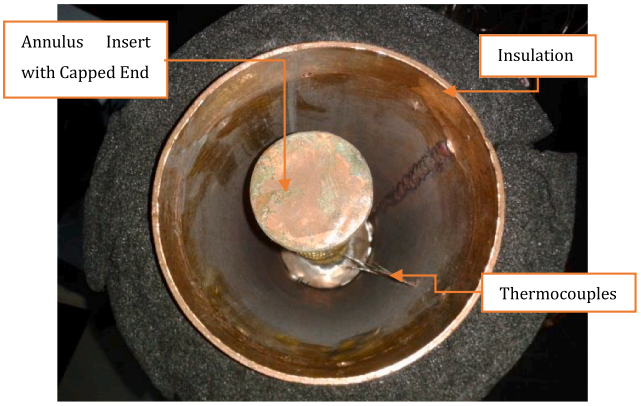

Fig. 2d. Cross-section of the Insulated Packed Bed Vessel with Annulus Insert

The integrated system was then set up by connecting it to the mixing box that generated the required moist air condition for the adsorbing bed (See Figs. 3a & 3b). At the inlet and outlet of the packed bed adsorber, sensors were placed to measure the inlet and outlet air velocity, temperature, relative humidity, and pressure. Here, the AZ8829 data loggers were used to record the inlet and outlet relative humidity (RH) and temperature. They were inserted in flexible pipes connecting the inlet and outlet of the adsorbing bed as shown in Fig. 3b. The

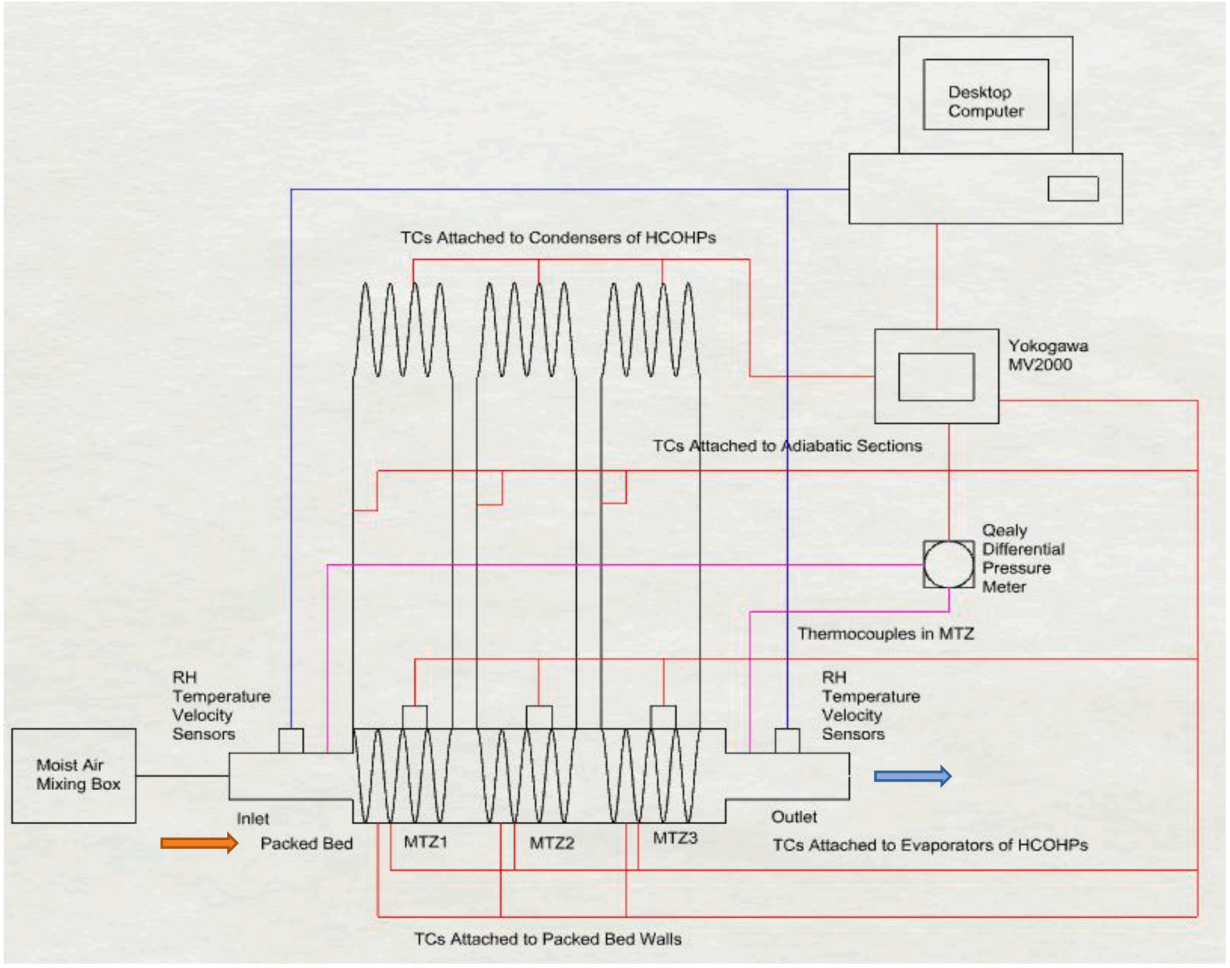

Fig. 3a. Schematic of the Integrated Packed Bed-HCOHP System.

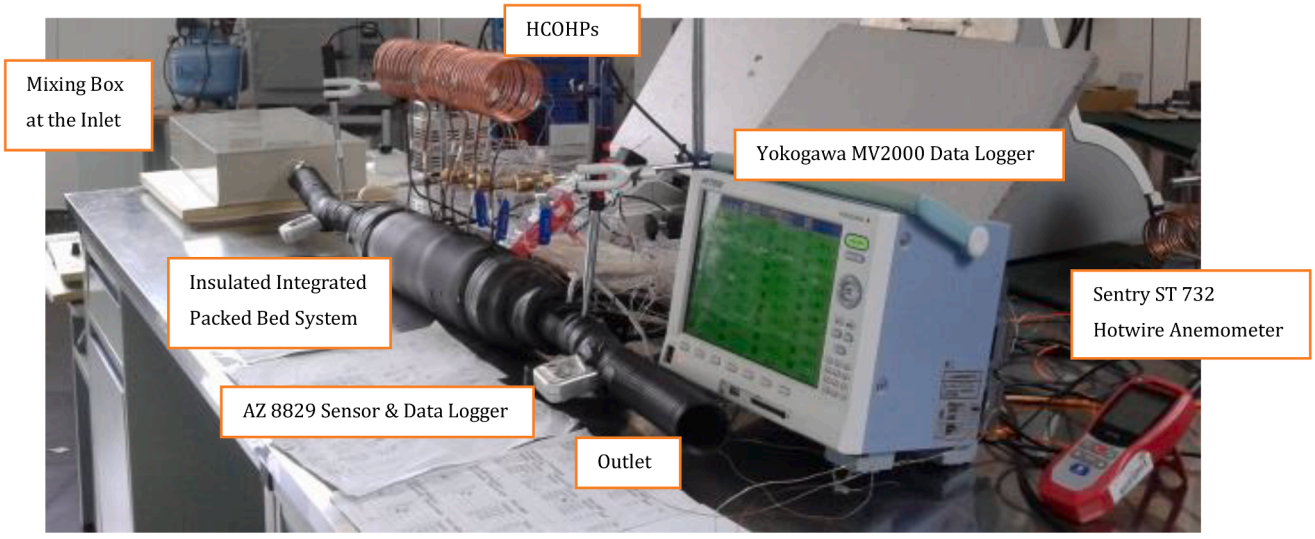

Fig. 3b. Experimental Setup of the Integrated Packed Bed-HCOHP System

temperature and relative humidity data were downloaded by connecting the AZ8829 data loggers to the personal computer (PC) via a docking station. The Sentry ST732 Hotwire Anemometer an air velocity, temperature of air, and non-contact infrared temperature measuring instrument that combines hot wire and standard thermistor to deliver rapid and precise measurements even at low air velocity was used to collect the velocities and corresponding air temperatures at the inlet and outlet of the packed bed. The inlet and outlet pressure differential were obtained by connecting the QEALY differential pressure meter, a pressure measurement device incorporating two compartments connected to

tubes inserted in the inlet and outlet flexible connections to the packed bed. This differential pressure meter connected to the Yokogawa MV2000 Data Logger also incorporated an internal transducer that converted the differential pressure into electrical signals which was subsequently converted into Pascal's using a conversion factor. The mixing box was then connected to the packed bed inlet for the supply of moist air to the bed. The data loggers were configured to collect data at 5 s intervals.

The packed bed vessel was oriented horizontally whilst the HCOHPs integrated with it were oriented vertically such that their evaporators were at the bottom and the condensers at the top (See Figs. 3a and 3b). This was critical because for the HCOHPs, the effect of inclination angle essentially reflects the influence of gravity on them [38]. Qu et al. [38] for instance found that the effect of gravity cannot be ignored as they observed the best thermal performance at the vertical bottom heating mode orientation with thermal resistance increasing as their device moved towards horizontal orientation.

2.3. Experimental and derived data

2.3.1. The moist air condition

The average inlet moist air properties are presented in Table 1. The temperature and relative humidity were obtained from sensor measurements, however based on the averages of these values for the respective packed bed configurations, average specific volume, enthalpy, density and specific heat at constant pressure for the inlet were determined with data from CIBSE Guide C [39] and Eq. (1) obtained from Cengal and Ghajar [40].

$$h = c_p T \tag{1}$$

The saturated vapour pressure over water in kPa determined using the inlet temperature and Eq. (2) obtained from CIBSE Guide C [39] was used to determine the inlet moisture content.

$$\log p_g = 30.59051 - 8.2\log(\theta + 273.16) + 2.4804 \times 10^{-3}(\theta + 273.16) - [3142.31/(\theta + 273.16)] \tag{2}$$

Eq. (3) obtained from CIBSE Guide C [39] and Jones [41] was used to determine the moisture content (in kg/kg of dry air) of the saturated moist air. The dimensionless enhancement factor, f_s, value of approximately 1.004 at a barometric pressure of 101.325 kPa and a temperature of 0 °C was used [41].

$$\omega_s = \frac{0.62197 f_s p_g}{101.325 - f_s p_g} \tag{3}$$

Eq. (4) was then used to determine the moisture content of unsaturated moist air, kg/kg of dry air as outlined in CIBSE Guide C [39] and Jones [41].

$$\omega = \frac{RH \times \omega_s}{100} \tag{4}$$

2.3.2. Properties and characteristics of the silica gel particles for adsorption

Table 2 below shows the characteristics and properties of the silica gel (SiO_2) particles determined under laboratory conditions. The surface properties of the particles were determined using the Brunauer-Emmett-Teller (BET) method, a gas adsorption method widely used in the determination of the surface area of finely divided and porous materials [42]. This was done for a sample of silica gel particles of mass 0.5315 g using Nitrogen gas (N_2) at 77 K as the adsorptive. The analysis was undertaken using the Micromeritics ASAP 2020, a Surface Area and Porosity Analyser for a period of 12 h.

Thermal properties of the silica gel particles were determined using KD2 Pro, a battery-operated, menu-driven device that measures thermal conductivity and resistivity, volumetric specific heat capacity and thermal diffusivity. The measurement was carried out at 60 temperature points between 26.770 and 30.049 °C for samples of silica gel particles dried for about 3 h at a temperature of about 115 °C and left to cool afterwards. This was to ensure that any physisorbed water vapour was removed before measurement commenced. The specific heat capacity of the silica gel particles on the other hand was determined using a differential scanning calorimeter (DSC) EXSTAR SII DSC 6220 with a sample of sapphire in a vial used as reference. The material density and volume were determined using Quantachrome Ultra PYC 1200e gas pycnometer. This analysis was carried out using Helium gas at a pressure of about 120 kPa and analysis temperature of about 34 °C.

As shown in Table 2, a BET average pore width of 23.0775 Å is about 2.3 nm implying that the average pore width just moves into the mesoporous region of the IUPAC [6] classification of pores where pores sizes <2 nm are classified as micropores. This suggests that the pore widths of the selected silica gel ranged between the mesoporous and microporous regions. According to ASHRAE [3], IUPAC [6], IUPAC [42], and Thommes [43] sorption behaviour in micropores is dominated almost entirely by the interactions between fluid molecules and the pore walls hence micropores fill through a continuous process. While sorption behaviour in mesopores depends not only on the fluid-wall attraction, but also on the attractive interactions between the fluid molecules leading to the occurrence of multilayer adsorption and capillary condensation. The BET surface area of 600.887 m^2/g is also wide enough to enable high adsorptive capacity to be achieved [10,44]. Overall, the values obtained from the BET measurements, thermal property measurements and pycnometer measurements presented in Table 2 compares favourably with data on thermophysical properties of type A and type RD silica gels presented in Chua et al. [44].

Table 3 shows data for the mass of the silica gel conditioned for adsorption and the amount of moisture adsorbed for the individual unintegrated packed bed configurations and their integration with respective HCOHPs. In the conditioning of the silica gel, the particles were weighed, oven dried and weighed again before being randomly packed for the respective adsorption processes. The mass of moisture adsorbed by the silica gel was then determined from the mass of the silica gel before and after the respective adsorption processes.

Table 4 shows the masses, volumes and bulk densities of the individual packed bed configurations and their respective integrated systems. Due to the random packing of the silica gel of size ranging between 3.35 and 4.75 mm, the masses in the vessel varied slightly. It is important to note that although the masses and the bulk densities varied for each configuration, they were in typical ranges hence the variation was inconsequential to the bed performance subsequently determined.

Table 5 shows the dimensions of the packed bed and its accessories. For the annulus packed beds, the packing cross-sectional area is the difference between the inner cross-sectional area occupied by the annulus section and the cross-sectional area of the main packed bed vessel. For the mesh screens, their inner diameters were used to calculate its cross-sectional area.

Table 6 shows the volumes and surface areas of the packed bed and its annulus configurations.

Table 7 shows the general dimensions of each of the HCOHPs used in the investigation.

3. Results and discussion

The results presented here are part of consistent results obtained from several experimental measurements carried out in the laboratory. The results typically show the performance difference between the respective integrated packed bed–HCOHP system and that of its corresponding unintegrated packed bed system.

3.1. Thermal contact resistance

The integrated packed bed-HCOHP system consisted of a cylindrical packed bed vessel pushed through the helically coiled oscillating heat pipe (HCOHP) evaporator coils in order to gain contact for heat transfer.

Table 1
Average inlet moist air properties.

Bed Type	Inlet Temperature, °C	Inlet Relative Humidity %	Inlet Moisture content of unsaturated moist air (kg/kg of dry air)	Specific Volume, m^3/kg_{da}	Density, kg/m^3	Enthalpy, kJ/kg	Specific Heat at Constant Pressure,c_{pw}, kJ/kg•K	Comments
FPB	29.05	86.25	0.0098	0.8841	1.1311	82.29	2.8326	Enthalpy and Specific Volume interpolated linearly using data from CIBSE Guide C [39].c_p calculated from Eq. (1)
FPB-EOHP	21.64	94.04	0.0089	0.8547	1.1700	60.31	2.7870	
FPB-MOHP	23.55	88.83	0.0088	0.8618	1.1603	64.77	2.7502	
FPB-WOHP	23.21	88.71	0.0087	0.8594	1.1635	62.72	2.7020	
LAPB	28.14	88.52	0.0098	0.8818	1.1340	82.54	2.9342	
LAPB-EOHP	25.74	80.88	0.0085	0.8702	1.1492	71.86	2.7911	
LAPB-MOHP	25.10	88.39	0.0092	0.8682	1.1518	70.33	2.8019	
LAPB-WOHP	22.89	85.85	0.0084	0.8552	1.1694	58.43	2.5522	
MAPB	27.62	93.06	0.010	0.8807	1.1355	82.52	2.9877	
MAPB-EOHP	25.99	88.05	0.0093	0.8727	1.1459	74.23	2.8559	
MAPB-MOHP	24.90	88.94	0.0092	0.8680	1.1521	69.95	2.8097	
MAPB-WOHP	21.52	88.81	0.0084	0.8533	1.1720	57.62	2.6767	
SAPB	28.23	85.62	0.0096	0.8710	1.1364	79.08	2.8013	
SAPB-EOHP	25.87	87.52	0.0093	0.8706	1.1486	72.62	2.8070	
SAPB-MOHP	23.12	86.29	0.0085	0.8578	1.1657	57.65	2.4937	
SAPB-WOHP	23.02	89.96	0.0088	0.8589	1.1643	61.68	2.6790	

Table 2
Properties and characteristics of the silica gel particles determined in the laboratory.

Parameter	Value	Units	Comments
BET Measurements from the Micromeritics ASAP 2020			
BET Surface Area	600.89	m^2/g	Nitrogen(N_2) gas Adsorptive, Analysis Bath Temperature = −195.82 °C
BET Pore Volume	0.35	cm^2/g	Sample mass analyzed = 0.5315 g Single point adsorption total pore
BET Average Pore Width	23.08	Å	volume of pores. At p/p^o = 1.001964
Thermal Property Measurements from the KD2 Pro			
Thermal Conductivity	0.20	W/m·K	Temperature range = 26.770–30.049 °C Error Margin 0.0007
Thermal Resistivity	506.70	°C·cm/W	
Thermal Diffusivity	0.12	mm^2/s	
Volumetric Specific Heat	1.70	MJ/m^3·K	
Specific Heat Capacity	1047.24	J/kg	Determined using EXSTAR SII DSC 6220 differential scanning calorimeter (DSC) Vial containing a sample of sapphire used as reference.
Pycnometer Measurements from the Quantachrome Ultra PYC 1200e			
Average Volume	31.13	cc	Helium gas at a pressure of about 120
Average Density	2.32	g/cc	kPa, Analysis temperature ≈34 °C Volume Standard Deviation (cc) = 13903, Density Standard Deviation (g/cc) = 0.1053 Coefficient of Variation % = 4.4667, Requested Deviation % = 0.0100 Achieved Deviation % = 3.9048

According to Fletcher and Gyorog [45] contact conductance varies considerably, depending upon the mechanical and thermophysical properties of the materials composing the contact, the surface conditions, and the interstitial fluid or filler. For this integrated packed bed-HCOHP system, the thermal contact resistance was previously evaluated in Yeboah and Darkwa [32] at different input temperatures and found to typically vary with working fluid type owing to respective effective thermal conductivities and conditions on the surfaces of contact. Using Eqs. (5) and (6) in Zhang et al. [46], the thermal contact resistances between the HCOHPs and the walls of the packed bed vessels were evaluated.

$$R_c = \frac{T_v - T_{evap}}{q_{av}} \tag{5}$$

$$q_{av} = \frac{q_v + q_{evap}}{2} \tag{6}$$

Figs. 4a–d shows the transient thermal contact resistance between the various HCOHPs integrated with the various packed bed configurations. It is important to note that the adsorption process is not linear as the heat from the packed bed reaches its peak and subsequently declines. As can be observed on the plots, the thermal contact resistances varied between different HCOHPs integrated with different packed bed

Table 4
Packed bed volume and silica gel bulk density.

Packed Bed	Mass of Silica Gel, g	Volume, m^3	Bulk Density kg/m^3
FPB	1099.00	0.00143	768.53
FPB-EOHP	1123.02		785.33
FPB-MOHP	1111.86		777.52
FPB-WOHP	1106.64		773.87
LAPB	881.71	0.00113	780.27
LAPB-EOHP	882.13		780.65
LAPB-MOHP	874.35		773.76
LAPB-WOHP	853.26		755.10
MAPB	903.18	0.00122	740.31
MAPB-EOHP	913.89		749.10
MAPB-MOHP	928.88		761.38
MAPB-WOHP	901.56		738.98
SAPB	987.90	0.00131	754.12
SAPB-EOHP	979.49		747.70
SAPB-MOHP	994.81		759.40
SAPB-WOHP	982.82		750.24

Table 3
Silica gel conditioning data.

Packed Bed Type	Silica Gel Mass Before Oven Drying, g	Oven Drying Temperature, °C	Oven Drying Time, hrs	Silica Gel Mass After Oven Drying, g	Silica Gel Mass After Adsorption, g	Total Mass of Moisture Adsorbed, g	Experimental Data Sampling Time (s)	Equivalent Adsorbed Moisture (g) at 2000 Data Sampling Time
FPB	1190.00	140	~3.5–4	1099.00	1263.00	164.00	7560	43.39
FPB-EOHP	1224.75	140	~3.5–4	1123.02	1169.65	46.63	2092	44.58
FPB-MOHP	1222.73	140	~3.5–4	1111.86	1160.31	48.45	2778	34.88
FPB-WOHP	1232.69	140	~3.5–4	1106.64	1151.04	44.40	2695	32.95
LAPB	996.21	140	~3.5–4	881.71	932.65	50.94	2513	40.54
LAPB-EOHP	947.73	140	~3.5–4	882.13	932.11	49.98	2180	45.85
LAPB-MOHP	968.72	140	~3.5–4	874.35	969.95	95.60	2669	71.64
LAPB-WOHP	929.45	140	~3.5–4	853.26	953.69	100.43	3093	64.94
MAPB	1012.64	140	~3.5–4	903.18	1017.43	114.25	2752	83.03
MAPB-EOHP	1090.81	140	~3.5–4	913.89	999.83	85.94	2395	71.77
MAPB-MOHP	1024.53	140	~3.5–4	928.88	1009.64	80.76	2719	59.40
MAPB-WOHP	1006.29	140	~3.5–4	901.56	987.05	85.49	2753	62.11
SAPB	1076.60	140	~3.5–4	987.90	1091.97	104.07	3189	65.27
SAPB-EOHP	1101.48	140	~3.5–4	979.49	1077.95	98.46	3017	65.27
SAPB-MOHP	1085.34	140	~3.5–4	994.81	1101.94	107.13	3411	62.81
SAPB-WOHP	1128.78	140	~3.5–4	982.82	1095.82	113.00	3405	66.37

Table 5
Dimensions of the fabricated packed bed vessel and its accessories.

Component	Length (cm)	Inner Diameter (cm)	Outer Diameter (cm)	Cross-Sectional Area (cm^2)
Packed Bed Vessel	35	7.8	8	47.78
Large Annulus Section	29	3.6	4	37.60
Medium Annulus Section	28	3.0	3.4	40.72
Small Annulus Section	28.4	2.3	2.6	43.63
Mesh Screen 1	–	6.6	7.7	34.21
Mesh Screen 2	–	6.5	7.7	33.18

Table 6
Packed volume and surface area.

Packed Bed	Packed Bed Volume, m^3	Packed Bed Surface Area m^2
FPB	0.0014	0.08
LAPB	0.0011	0.11
MAPB	0.0012	0.11
SAPB	0.0013	0.10

Table 7
HCOHP dimensions.

Parameter	Value	Units
Inner Diameter	2	mm
Thickness	1	mm
Diameter of Coil	8	cm
Length of Compressed Coil	10	cm
Number of Turns	10	–
Length of Adiabatic Section	20	cm
Total Length of HCOHP	38	cm
Area of Evaporator/Condenser,A_e/A_c	0.02	m^2
Length of Evaporator/Condenser,L_e/L_c	0.19	m

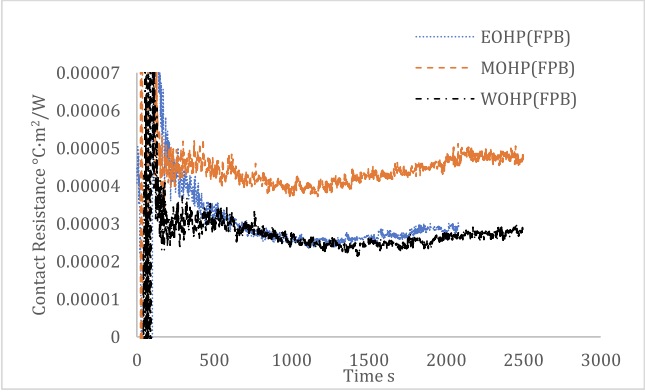

Fig. 4a. Thermal Contact Resistance for Integrated FPB-HCOHP

configurations largely due to the HCOHP working fluid type, amount of heat generated by the packed bed and the surface condition of the contacts. Apart from integration with the Large Annulus Packed Bed (LAPB), the deionised Water Oscillating Heat Pipe (WOHP) consistently exhibited a comparatively lower thermal contact resistance between its evaporator and the walls of the packed beds it was integrated with. The Methanol Oscillating Heat Pipe (MOHP) on the other hand showed a comparatively higher transient thermal contact resistance in all its integrated systems as shown in Fig. 4. It is important to note that both the

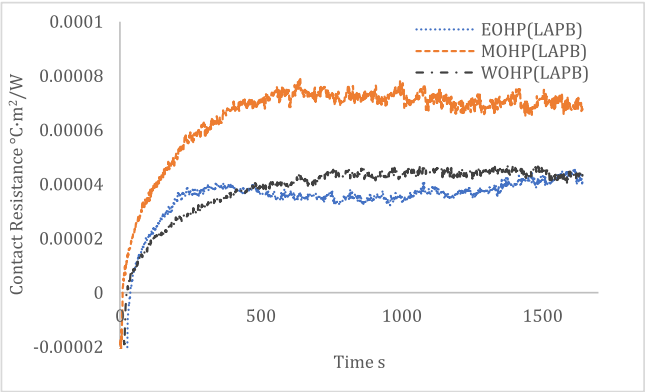

Fig. 4b. Thermal Contact Resistance for Integrated LAPB-HCOHP

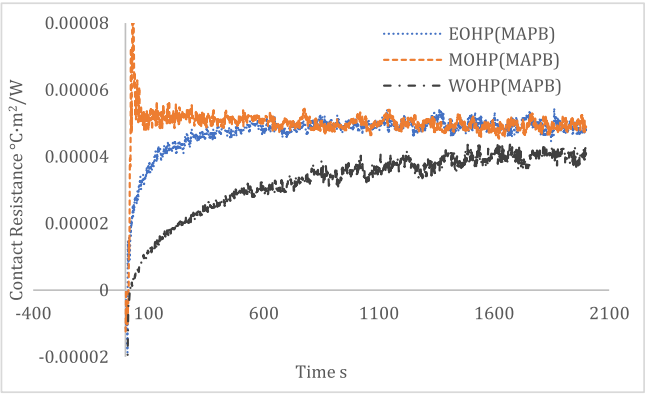

Fig. 4c. Thermal Contact Resistance for Integrated MAPB-HCOHP

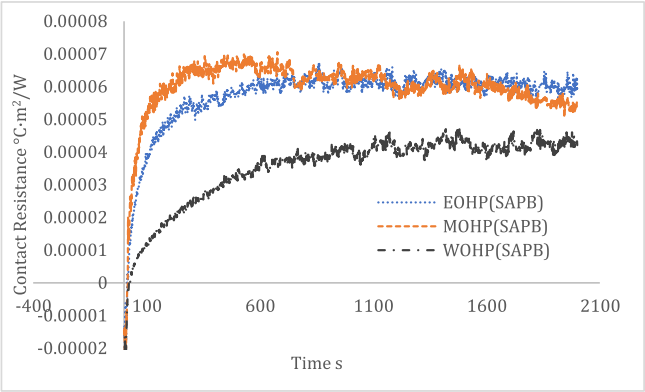

Fig. 4d. Thermal Contact Resistance for Integrated SAPB-HCOHP

HCOHPs and the packed bed vessels were made from copper of similar surface roughness purchased from the open market. Holman [47] estimates a typical surface roughness of 3.81 μm for milled copper of this kind.

In Table 8 the averages of the thermal contact resistances determined between the various packed bed configurations and the HCOHPs along with the average heat input into the evaporators are presented. For the integrated systems investigated, the average values in Table 8 show variation in average thermal contact resistances and average heat input into the evaporator from the packed beds. The evaporator heat inputs were determined using the temperature difference between packed bed and its wall. It was observed here that though the average thermal contact resistance varied with heat input, it was not a linear relationship

Table 8
Average evaporator heat input and average thermal contact resistances between packed beds and HCOHPs.

Packed Bed Configuration	HCOHP Type and Evaporator Heat Input					
	Heat Input, W	EOHP, C·m^2/W	Heat Input, W	MOHP, C·m^2/W	Heat Input, W	WOHP, C·m^2/W
FPB	37.13	2.94×10^{-05}	32.44	4.40×10^{-05}	34.04	3.05×10^{-05}
LAPB	40.73	2.67×10^{-05}	31.68	6.60×10^{-05}	46.47	3.90×10^{-05}
MAPB	36.04	4.71×10^{-05}	34.70	4.99×10^{-05}	34.32	3.20×10^{-05}
SAPB	31.14	5.71×10^{-05}	32.13	5.98×10^{-05}	36.65	3.52×10^{-05}

and it did not mimic the profile of the heat outputs from the packed beds. Comparatively large average thermal contact resistance values were determined for the MOHP consistent with the transient profiles. The WOHP on the other hand was found to have similar average thermal contact resistance values in all integrated systems unlike the Ethanol Oscillating Heat Pipe (EOHP) and Methanol Oscillating Heat Pipe (MOHP) which showed significant variations depending on the packed beds they were integrated with.

The thermal contact resistances observed here shows that thermal conductance was dependent on the amount of heat from the vessel, the working fluid type and other surface conditions. For the working fluids chosen, it is well established in literature [40] that their typical thermal conductivities are in the order of $H_2O(0.556W/m\cdot K) > CH_3OH(0.204W/m\cdot K) > C_2H_5OH(0.171W/m\cdot K)$. Although ethanol has a comparatively lower thermal conductivity, higher averages of thermal contact resistances was recorded for the MOHP integrated systems instead implying that other factors may be dominant. As outlined by Fletcher and Gyorog [45] there may be other conditions and factors not necessarily monitored in this study such as the variation in the gaps between contact surfaces due to limitations in fabrication and varying surface roughness resulting in resistance to heat transfer between the evaporator coils and the packed bed vessel walls.

Overall, thermal contact resistance between the coils of the HCOHP and the walls of the packed bed vessel varied nonlinearly with the amount of heat from the vessel as it did not mimic the adsorption heat output profile from the packed beds. It was observed to be higher in the MOHP than the EOHP although ethanol has a lower thermal conductivity than methanol implying that other factors were dominant to the resistance to the heat transfer.

3.2. Thermal performance of the HCOHPs

The thermal performance of the HCOHPs integrated with the various packed bed configurations were evaluated. The heat from the packed beds transferred through the walls of the copper vessel was determined as the heat input to the evaporators using the Fourier's Eq. (7) [48]. Here, it was assumed that the inner walls of the copper vessel received the total amount of heat generated by the packed silica gel via heat of adsorption and this heat was transferred via conduction to the outer walls of the copper vessel.

$$q_w = -kA_s\frac{dT}{dr} = 2\pi \mathrm{Lk}\frac{T_i - T_o}{\ln(r_o/r_i)} \tag{7}$$

The thermal performance of the integrated system was evaluated by determining the overall thermal resistance (R) using Eq. (8) obtained from Hao et al. [49].

$$\mathrm{R} = \frac{\overline{T}_e - \overline{T}_c}{Q} \tag{8}$$

The heat generated by the packed silica gel beds varied with the packed bed configuration. As shown in Table 4, the slight variations in bulk densities for each packed bed configuration influenced the amount of heat generated by the beds albeit inconsequential to the overall adsorption performance. It is important to note that the adsorption process is not linear as the higher rate of adsorption occurs during the first few minutes resulting in the heat generation rate rapidly increasing the bed temperature [37] before subsequently declining. For this reason, it is critical to focus on the performance of the HCOHPs in the first few minutes as that is significant on the overall thermal performance of the integrated system. The working fluids for the HCOHPs as shown in Yeboah and Darkwa [32] were chosen to be in the useful temperature range of the adsorption process.

3.2.1. Start-Up behaviour

Start-up behaviour of PHPs/OHPs is found to be dependent on the type of working fluid [38]. In this investigation, start-up for each HCOHP was found to vary with evaporator heat input amount and the working fluid type. For the same HCOHPs integrated with different packed bed configurations, start-up was found to vary with heat input amount as shown in Figs. 5a–d. For the annulus packed bed configurations, the HCOHPs start-up required between 2.1 W and 7.4 W of heat input to the evaporators over various time ranges. For the Fully Packed Bed (FPB) configuration in Fig. 5a, start-up was relatively unstable until after about 50 s. Here, the heat input initially rose to a local maximum before declining to a local minimum. As shown in Fig. 5a the evaporator heat input increased from respective local minima before the ascent of the heat input over time indicating start-up of the HCOHPs. It is worthy to note that this random and fully packed configuration is subject to flow mal-distribution so the instabilities observed around start-up could be as a result of irregular fluid–solid contact at the early stages when the moist air flowed through the bed. Per the mass of silica gel packed within it, more heat should be released, however the mal-distribution of flow reduced the amount of fluid solid contact that releases the heat of adsorption.

For the HCOHPs integrated with the annulus packed beds presented in Figs. 5b–d, start-up varied at different evaporator heat inputs. For the MOHP start-up was gradual when integrated with the Medium Annulus Packed Bed (MAPB) and Small Annulus Packed Bed (SAPB) but was sudden as shown by the steep inclination of the heat input profile when integrated with the Large Annulus Packed Bed (LAPB), the configuration with a comparatively lower heat output. For the EOHP and WOHP, start-up took relatively longer (beyond 15 s) when integrated with the LAPB configuration and were both relatively quicker (around 10 s) when integrated with the MAPB and SAPB configurations, both with comparatively higher heat outputs than the LAPB. For the WOHP, start-up occurred when heat input was between 5.7 W and 6.3 W for the various annulus configurations. For the EOHP and MOHP, a comparatively wider range was observed. For the EOHP start-up heat input started from

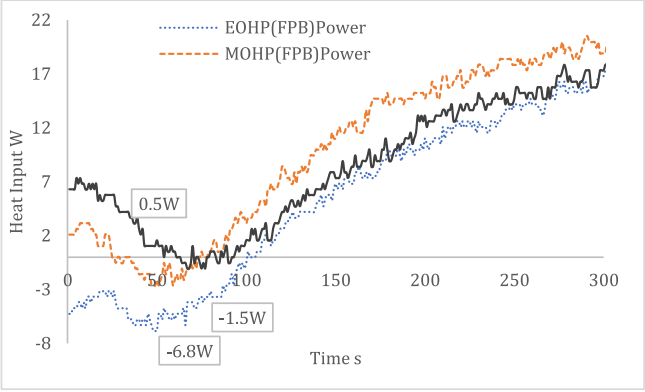

Fig. 5a. Integrated FPB-HCOHP Start-up

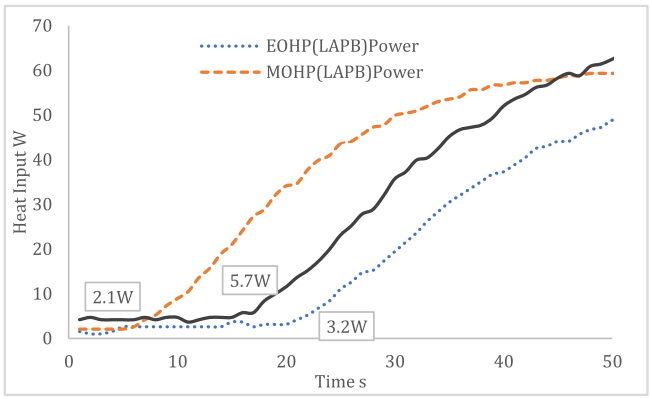

Fig. 5b. Integrated LAPB-HCOHP Start-up

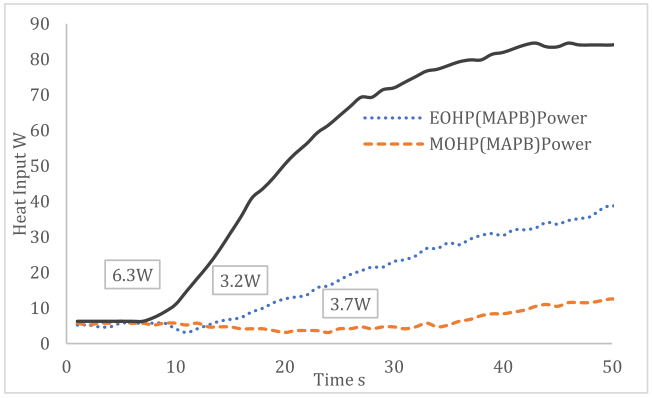

Fig. 5c. Integrated MAPB-HCOHP Start-up

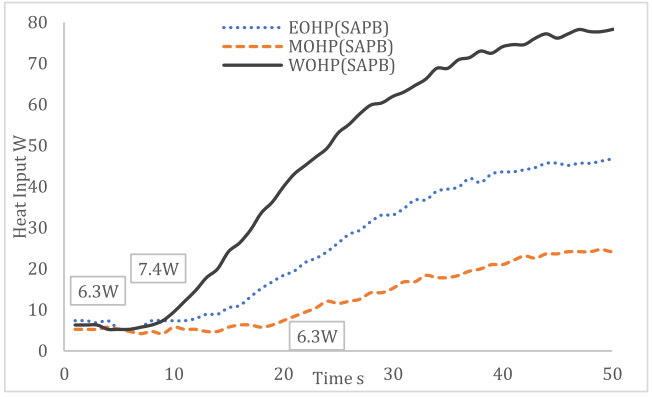

Fig. 5d. Integrated SAPB-HCOHP Start-up

3.2 W to7.4 W while for the MOHP it was from 2.1 W to 6.3 W. For all configurations, the HCOHPs required less than 10 W of input power for the evaporators to start-up.

For an evacuation pressure of about 0.0013 MPa, the boiling points for ethanol, methanol, and water in the HCOHPs significantly reduced. Using the Clausius–Clapeyron relation, the boiling points of ethanol, methanol and water were determined to be around −8.5 °C, −22.3 °C and 6.9 °C respectively at the determined evacuation pressure of 0.0013 MPa and standard pressure around 101.325 kPa. This implies that once the fluids in the HCOHPs reached those temperatures under that pressure, boiling should occur resulting in the oscillation of the working fluids in the HCOHPs. The observed delay in start-up of the HCOHPs can be attributed to several possible factors including the rate of heat transfer from the silica gel packing to the walls of the packed bed vessel, differences in conductivities of the materials (air, silica gel, copper and the respective working fluids), and the resistance to heat transfer between the evaporator walls and the packed bed vessel etc. Within the vessel, the random nonuniform packing is known to influence the heat transfer within the bed as near the walls the wall effect exists [15]. The thermocouple locations inside the packed beds and on the walls of the vessel provided a temperature difference as shown in Figs. 6a–d. This temperature difference was influenced by material (air, silica gel and copper) thermal conductivities and wall channelling due to the random packing. In Fig. 6a, it can be observed that the start-up of HCOHPs resulted in the flattening of the bed wall temperature difference curves for the integrated FPB-HCOHP systems. Here, the rise in temperature of the bed at the early stages of adsorption observed in the unintegrated packed bed was quelled by the HCOHPs when the FPB was integrated with them. For the annulus packed beds, the delay in start-up observed for some of the HCOHPs is evident in the profiles in Figs. 6b–d. For instance, the comparatively slow start-up of the WOHP can be seen in the relatively large bed to wall temperature difference at the early stages of the adsorption process. It is important to recognize that the working fluid in the WOHP under the evacuation pressure of about 0.0013 MPa had a boiling point of 6.9 °C comparatively higher than that of the EOHP and MOHP. For the annulus packed beds in Figs. 6b–d, the differences in start-up of the HCOHPs is reflected in the different peak adsorption temperatures at the early stage of the adsorption process.

The start-up of the HCOHPs was critical to the integrated system performance due to the exothermic nature of the adsorption process making the heat from the packed bed peak at the early stages and declining subsequently.

3.2.2. *Heat input and overall thermal resistance*

The evaporator heat input and the overall thermal resistance for the HCOHPs integrated with the various packed beds are presented in Figs. 7–10. The legend for the evaporator heat input power ends with Power while that of the overall thermal resistance ends with TR. From Fig. 7 the transient evaporator heat input obtained from the copper vessel determined using Eq. (7) and the overall thermal resistance obtained from Eq. (8) are presented for the integrated FPB-HCOHP system. The general trend shows that as the heat input increases the overall thermal resistance decreases. It can be seen on the plots that the maxima of the heat input power coincide with the minima of the overall thermal resistance. Since the adsorption heat generated increases to a peak and subsequently declines, it can be observed that as the heat input decreases the overall thermal resistance increases. It is important to note that the random fully packed configuration of the FPB resulted in the mal-distribution of flow within the bed leading to ineffective fluid solid contact.

The averages of the overall thermal resistance determined for the HCOHPs integrated with the FPB packed bed configuration were

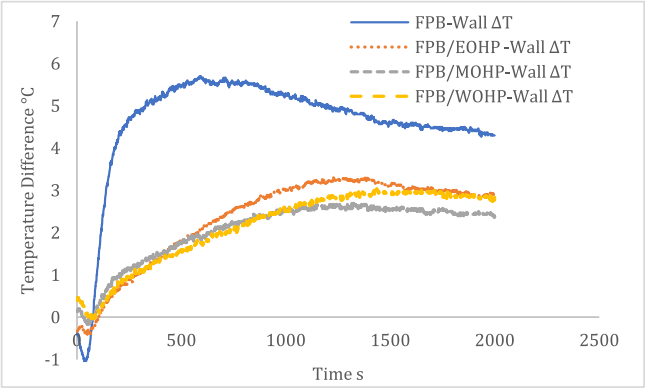

Fig. 6a. FPB Bed-Wall Temperature Difference

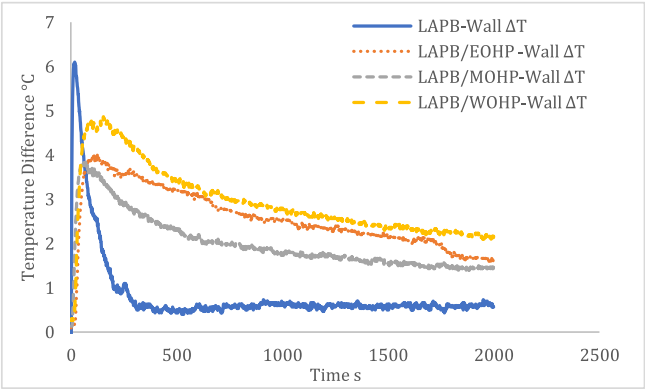

Fig. 6b. LAPB Bed-Wall Temperature Difference

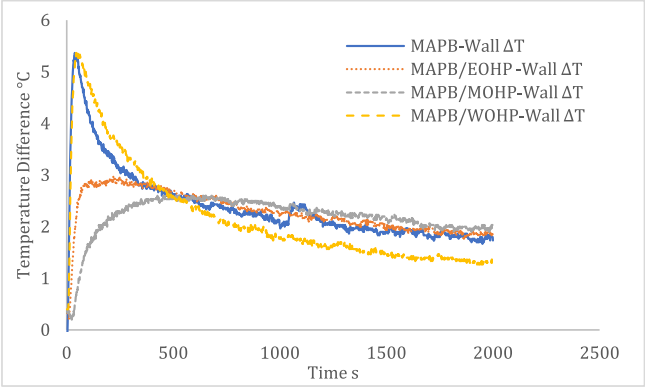

Fig. 6c. MAPB Bed-Wall Temperature Difference

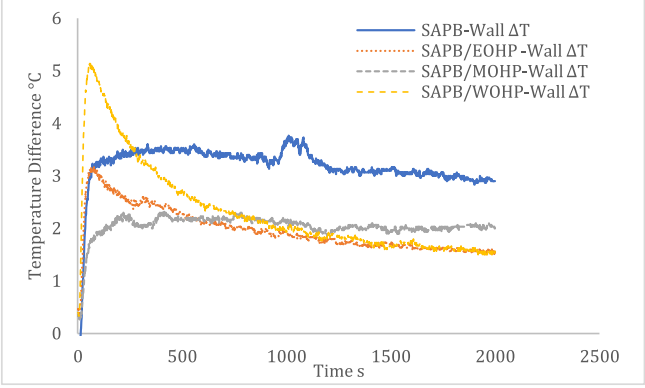

Fig. 6d. SAPB Bed-Wall Temperature Difference

0.14 °C/W, 0.18 °C/W and 0.17 °C/W respectively for the EOHP (FPB), MOHP (FPB) and WOHP (FPB). At its peak, the maximum heat inputs observed at the evaporators were 41.0 W, 45.7 W and 52.0 W for the MOHP, WOHP and EOHP, respectively. Significant instabilities in the thermal performances of the HCOHPs were observed at the early stages when the corresponding heat input was below about 10 W. Over time the MOHP was observed to have the worst performance of the three HCOHPs as its overall thermal resistance soared. The EOHP and WOHP showed identical performances after about 1600 s when they both had relatively similar heat input of around 47 W into their evaporators. Overall, at peak heat input, which is also the peak of the adsorption process, the EOHP performed significantly better than the WOHP and the MOHP for this integrated system.

As distinctive of the physical adsorption process, the heat input to the evaporator rose to the peak for each integrated LAPB-HCOHP system respectively before suddenly declining to lower values as shown in Fig. 8. At the point where the heat input was at the maximum, the HCOHPs were basically starting up. The LAPB configuration has the smallest mass of silica gel packing and its annulus structure offers a comparatively better uniform distribution of flow within this packed bed configuration for enhanced physical adsorption. For this reason, there was effective fluid–solid contact to ensure peak adsorption at the early stages which implied a significant and quick realisation of peak heat output from the silica gel bed. The variation in peak adsorption heat input to the evaporators here was largely due to the start-up performance of the HCOHPs. Due to its comparatively smaller silica gel mass, the physical adsorption process reached saturation quickly with the heat output from this packed bed configuration correspondingly declining. So as the heat output declined, it was observed that the transient overall thermal resistance increased indicating that the HCOHPs performed relatively poorly at lower evaporator heat inputs. From Fig. 8, the peak heat input power to the evaporator was 63 W for the EOHP, 59.4 W for the MOHP and 76.2 W for the WOHP. The corresponding averages of the overall thermal resistance were 0.13 °C/W, 0.27 °C/W and 0.15 °C/W for the EOHP (LAPB), MOHP (LAPB) and WOHP (LAPB) respectively. For this packed bed configuration, the MOHP appears to perform poorly as the average heat input was comparatively lower. This is corroborated in Yeboah and Darkwa [33] where the LAPB was the only configuration found to have the lowest average heat output. The MOHP obtaining a comparatively higher overall thermal resistance implies its relatively lower performance at comparatively lower evaporator heat input than the EOHP and WOHP. This goes to suggest that the parameters of the system have to be optimized in a bespoke manner to achieve optimum performance of the integrated system.

The MAPB configuration has a comparatively larger mass of silica gel and a relatively smaller annulus dimension than the LAPB system as shown in Table 4. In Fig. 9 the MAPB integrated system shows a sharp rise to the peak of adsorption and a rapid decline in heat output. This phenomenon is consistent with what was observed for the LAPB integrated system as the annulus configuration increased the fluid solid contact at the early stages hence reaching saturation relatively quickly. The heat input to the evaporator reached its maximum at the early stages of adsorption when start-up of the HCOHPs had barely begun. The subsequent decline in the heat output from the bed when adsorption approached saturation resulted in a decline in evaporator heat input and subsequent increase in the transient overall thermal resistance. What is obvious here is the fact that the performances of the integrated systems varied at the peak temperatures. This may be put down to start-up of the HCOHPs. For instance, for the WOHP (MAPB) integrated, although the maximum bed temperature was recorded here, the WOHP was able to overall reduce the bed temperature significantly more than the EOHP and the MOHP. The variation in the peak evaporator heat input at the early stages signifies more the start-up performance of the HCOHPs than their overall thermal performance. In fact, averaging the transient overall thermal resistance shows that their performances when integrated with this packed bed configuration was similar. The average overall thermal resistances for the EOHP, MOHP and WOHP were determined to be respectively 0.23 °C/W, 0.22 °C/W and 0.23 °C/W. However, it was also observed that the HCOHPs reduced the heat output from the MAPB to varying degrees though their performances were similar.

The trends for SAPB integrated systems were similar to that of the LAPB and the MAPB. For this packed bed, Yeboah and Darkwa [33] observed that although the annulus section improved the flow distribution within it, the relatively large mass of randomly packed silica gel limited effective fluid–solid contact as observed in the LAPB and MAPB configurations. In Fig. 10, variation in the peak evaporator heat inputs of the integrated SAPB-HCOHP systems can be observed. Once again, the WOHP at start-up was incapable of reducing the peak heat output of the packed bed as was achieved with the EOHP and MOHP. Here, the WOHP

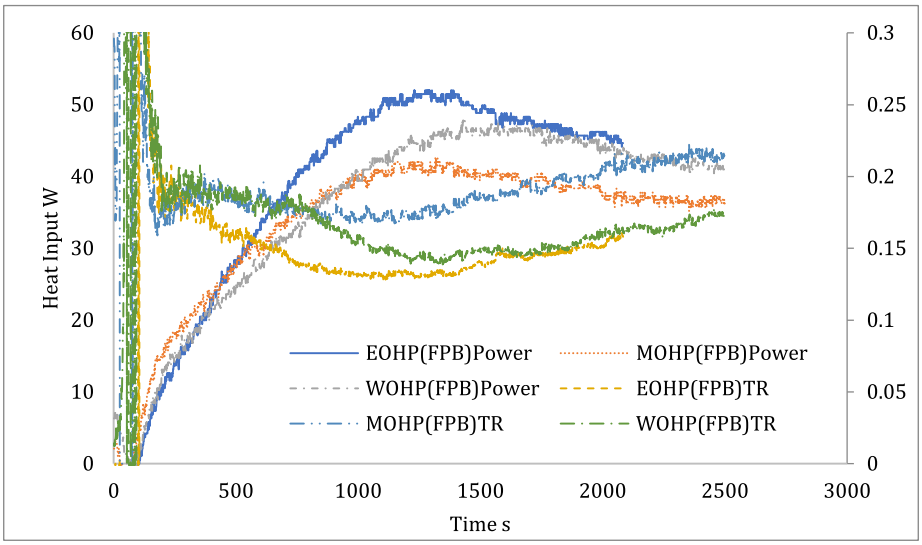

Fig. 7. Evaporator Heat Input and Overall Thermal Resistance for the HCOHPs Integrated with the FPB

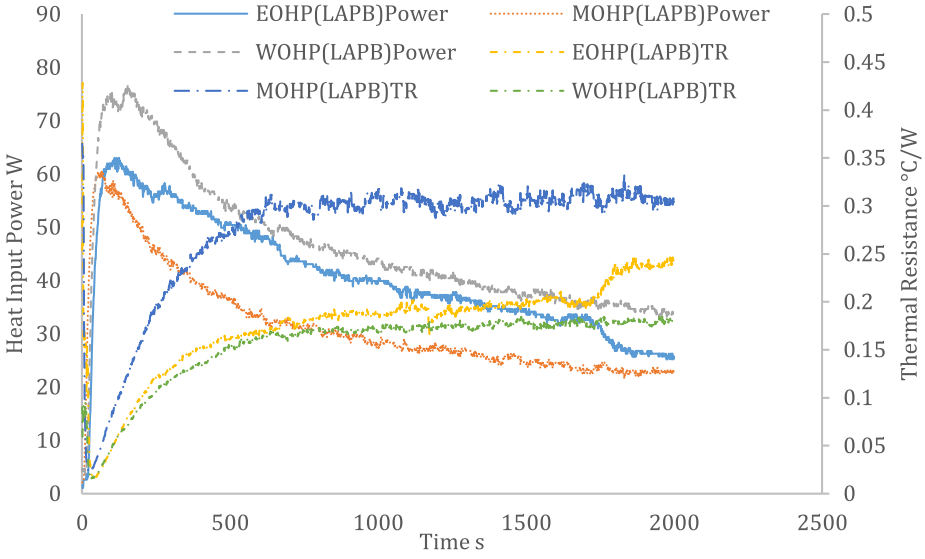

Fig. 8. Evaporator Heat Input and Overall Thermal Resistance for the HCOHPs Integrated with the LAPB

(SAPB) system had peak evaporator heat input of 80.9 W while the EOHP (SAPB) and MOHP (SAPB) systems recorded maximum peak evaporator heat inputs of 49.4 W and 35.7 W, respectively. For the MOHP (SAPB) integrated system, the profile shows that the MOHP was able to flatten the heat output from the packed bed immediately it reached its peak. For both the EOHP (SAPB) and WOHP (SAPB) integrated systems, it can be seen that the heat input reached its maximum before sharply declining. The thermal performance of the MOHP here appeared to be superior to that of the EOHP and WOHP. The averages of the overall thermal resistances were respectively 0.29 °C/W, 0.24 °C/W, and 0.25 °C/W for the EOHP, MOHP and WOHP showing a comparatively better thermal performance of the MOHP. The reason here is that as the heat output from this packed bed configuration sharply declined, the thermal performances of the EOHP and WOHP declined accordingly. However, for the MOHP, it managed to flatten the heat output to a relatively consistent value hence maintaining a relatively consistent transient thermal performance.

3.3. Packed bed heat transfer

3.3.1. Bed temperature distribution

The temperature distribution across the independent packed beds and corresponding integrated-HCOHP systems with references to their respective ambient temperatures are presented in Figs. 11–14. The condensers of the Helically Coiled Oscillating Heat Pipes (HCOHPs) were exposed to the ambient surroundings under standard atmospheric pressure of around 101.325 kPa. In the packed beds, Omega K type thermocouples were inserted in the designated mass transfer zones MTZ 1, MTZ 2 and MTZ 3 equidistance from each other. It is important to note that unlike the Fully Packed Bed (FPB), the temperature increase in the zone of mass transfer was counter flow to the inlet airflow direction for all the annular packed beds. This was due to the capped end of the annulus insert impeding the airflow and creating turbulent eddies around the capped ends subsequently driving radial air flow distribution within the bed [33]. As typical with water vapour adsorption on silica gel, the adsorption rates were maximum at the beginning resulting in the heat generation rate rapidly increasing the bed temperature [37]. Tables 9a–d shows the peak and average temperature values in the mass

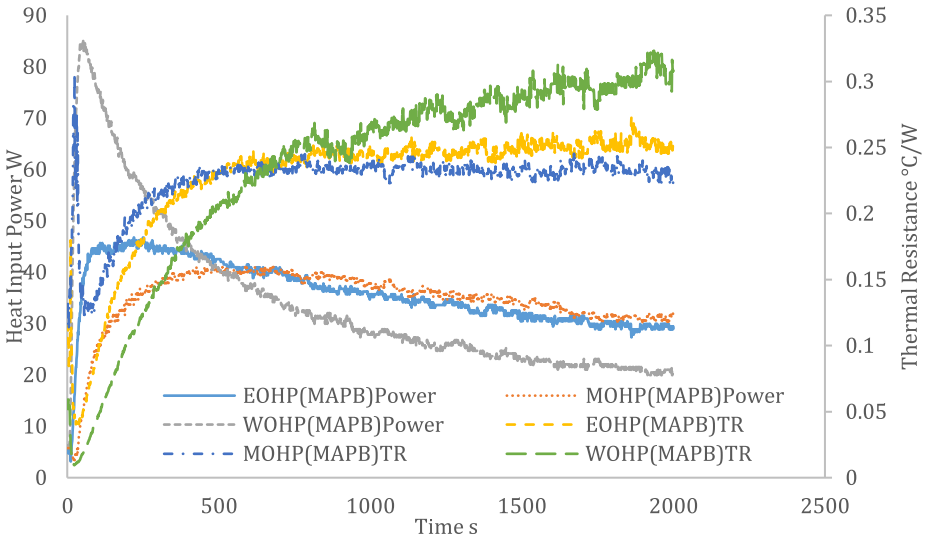

Fig. 9. Evaporator Heat Input and Overall Thermal Resistance for the HCOHPs Integrated with the MAPB

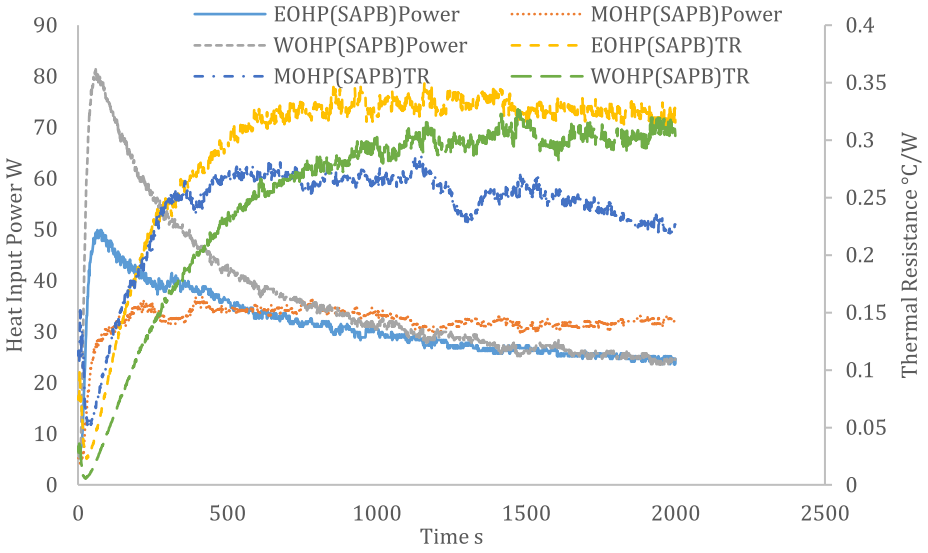

Fig. 10. Evaporator Heat Input and Overall Thermal Resistance for the HCOHPs Integrated with the SAPB

transfer zones for the independent packed beds and their corresponding integrated-HCOHP systems during the adsorption process.

In Figs. 11a–d, the temperature profiles of the FPB and its integrated systems follows the typical rise in temperatures observed in adsorption systems. As summarised in Table 9a, the peak adsorption and average bed temperatures decreased from MTZ 1 to MTZ 3. Between the independent FPB and its integrated systems, it is observed that the peak adsorption and average bed temperatures decreased on integration with the HCOHPs. MTZ 1 was the zone observed with the maximum temperature. Here peak adsorption temperature reduction of about 20 °C was obtained between the FPB and its respective integrated FPB-HCOHP systems. In this same mass transfer zone, average temperature differences between the FPB and its integrated FPB-HCOHP systems ranged between 17.7 °C and 18.7 °C. For the MTZ 3, the zone with the minimum peak and average temperatures, peak temperature reduction ranged between 10.4 °C and 13 °C for the FPB and its integrated FPB-HCOHP systems. While average temperature differences for this zone ranged between 10 °C and 11.7 °C for the FPB and its integrated FPB-HCOHP systems.

Here also, the performance of the EOHP integrated with this packed bed configuration appeared to be slightly better than that of the MOHP and WOHP integrated systems. It is important to note that with this fully packed configuration, the mal-distribution of flow was significant due to comparatively poor fluid–solid contact in the fully and randomly packed

Table 9a
Peak and Average Temperature Values (°C) in the Mass Transfer Zones for the FPB and its Integrated Systems.

Mass Transfer Zones	FPB		FPB-EOHP		FPB-MOHP		FPB-WOHP	
	Peak	Average	Peak	Average	Peak	Average	Peak	Average
MTZ 1	57.4	51.7	36.6	33.0	37.2	34.0	36.8	33.2
MTZ 2	43.5	38.4	30.3	26.8	32.3	28.4	29.8	26.9
MTZ 3	40.5	36.5	27.5	24.8	30.1	26.5	28.0	25.2

Table 9b
Peak and average temperature values (°C) in the mass transfer zones for the LAPB and its integrated systems.

Mass Transfer Zones	LAPB		LAPB-EOHP		LAPB-MOHP		LAPB-WOHP	
	Peak	Average	Peak	Average	Peak	Average	Peak	Average
MTZ 1	40.6	37.7	33.2	31.6	33.8	31.5	30.9	29.1
MTZ 2	42.7	39.3	33.1	31.3	35.4	32.7	32.3	30.2
MTZ 3	42.9	35.5	39.6	35.6	42.4	36.7	43.0	36.3

Table 9c
Peak and average temperature values (°C) in the mass transfer zones for the MAPB and its INTEGRATED SYStems.

Mass Transfer Zones	MAPB		MAPB-EOHP		MAPB-MOHP		MAPB-WOHP	
	Peak	Average	Peak	Average	Peak	Average	Peak	Average
MTZ 1	39.0	36.5	33.7	31.9	32.6	30.7	28.2	26.9
MTZ 2	41.1	38.2	34.8	32.6	33.9	31.7	29.2	27.6
MTZ 3	47.4	40.7	42.0	37.8	40.5	37.1	37.4	32.5

Table 9d
Peak and average temperature values (°C) in the mass transfer zones for the SAPB and its integrated systems.

Mass Transfer Zones	SAPB		SAPB-EOHP		SAPB-MOHP		SAPB-WOHP	
	Peak	Average	Peak	Average	Peak	Average	Peak	Average
MTZ 1	43.5	40.7	34.8	32.8	33.0	31.2	30.7	29.0
MTZ 2	43.3	39.7	35.5	33.1	32.9	30.9	32.1	30.1
MTZ 3	52.0	44.9	41.9	37.4	38.8	35.4	40.6	35.7

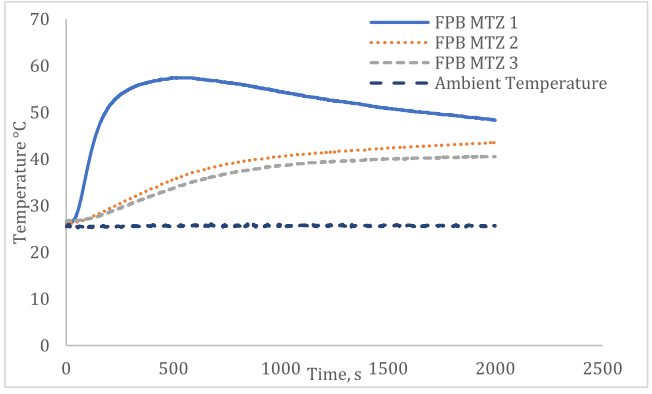

Fig. 11a. FPB Temperature Distribution Across Bed

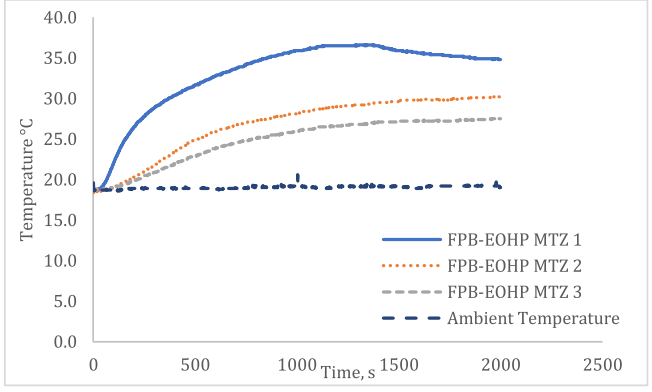

Fig. 11b. FPB-EOHP Temperature Distribution Across Bed

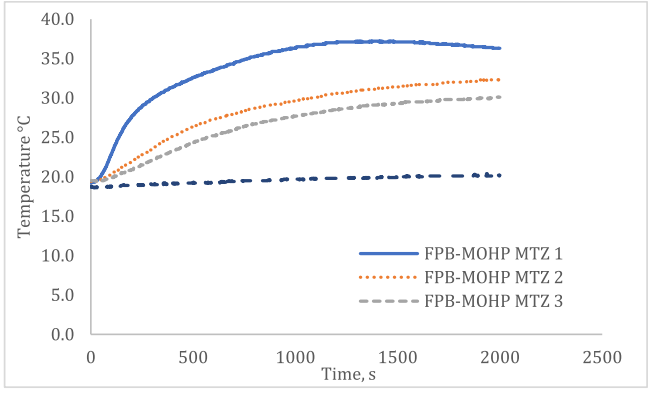

Fig. 11c. FPB-MOHP Temperature Distribution Across Bed

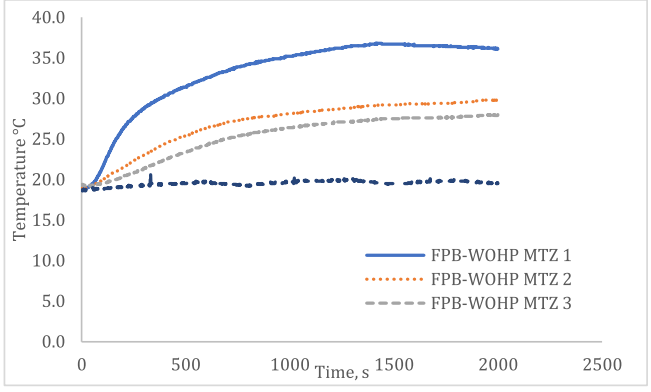

Fig. 11d. FPB-WOHP Temperature Distribution Across Bed

arrangement hence the significant difference in peak and average temperatures between the MTZ 1 and the other mass transfer zones [33]. The random nature of the packing also resulted in low outlet air velocities indicating high pressure drops and the requirement for significant fan power. This is affirmed by de Klerk [50] and Kabeel [51] who showed that bed parameters such as particle size and diameter to

bed depth ratio alters the pressure drop in the bed. According to de Klerk, particle size for instance does not only influence pressure drop in the bed but also the flow characteristics, filterability and adsorption kinetics.

Figs. 12–13 show the temperature profiles of the annulus packed beds and their corresponding integrated HCOHP systems. Heggs et al. [34] showed that annular structure can reduce the overall pressure drop although it will impact on residence time distribution of flow due to the annular packing matrix. Unlike the FPB, the zone of mass transfer here was counter-flow to the air flow direction.

Figs. 12a–d show the temperature profiles for the Large Annulus Packed Bed (LAPB) and its integrated systems, with Table 9b providing summaries of the peak and average temperatures in their corresponding mass transfer zones. The comparatively large annulus structure for this configuration increased fluid–solid contact for adsorption. As shown in Table 3 and 4, the mass of silica gel available for the adsorption process here was also comparatively smaller. This implied that the configuration allowed significant fluid–solid mixing which increased the adsorption rate leading to shorter equilibrium times. To this end the sharp increase in the temperatures especially in the MTZ 3, where significant adsorption begun at first, quickly declined as shown in Figs. 12a–d. It was also observed that the peak temperatures in the MTZ 3 for the LAPB and its integrated systems were relatively close implying that the effective fluid–solid mixing in this configuration led to a quick rise in temperature in this zone. The varying start-up of the HCOHPs may have resulted in this mass transfer zone achieving practically its maximum possible temperature irrespective of the integration of the HCOHPs. For instance, the MTZ 3 of the LAPB (WOHP) system and that of the LAPB system both achieved similar peak adsorption temperatures during the adsorption process indicating that the WOHP possibly had a delayed start-up. The relatively close peak temperatures observed for the LAPB-EOHP and LAPB-MOHP indicates that the fluid–solid mixing in MTZ 3 was effective hence the different start-up times of the HCOHPs only resulted in a maximum of 3 °C drop in the peak adsorption temperature. Over time, in subsequent mass transfer zones, the HCOHPs were observed to reduce the peak adsorption and average bed temperatures as shown in Table 9b as they would have been operational hence rejected heat to the ambient surroundings. For this reason, in MTZ 1 and MTZ 2, comparatively larger temperature differences in the peak adsorption and average bed temperatures were observed between the LAPB and its integrated systems. In these two mass transfer zones, the WOHP integrated system was observed to show optimal performance.

The Medium Annulus Packed Bed (MAPB) configuration has a slightly smaller annulus dimension than the LAPB($D_o/D_i = 2.35$). It also has a comparatively lager mass of silica gel particles than the LAPB as presented in Tables 3 and 4. For this reason, the level of fluid–solid contact was slightly diminished in the random packing hence equilibrium time was comparatively longer than that of the LAPB. Figs. 13a–d shows the temperature profiles of the MAPB and its integrated systems

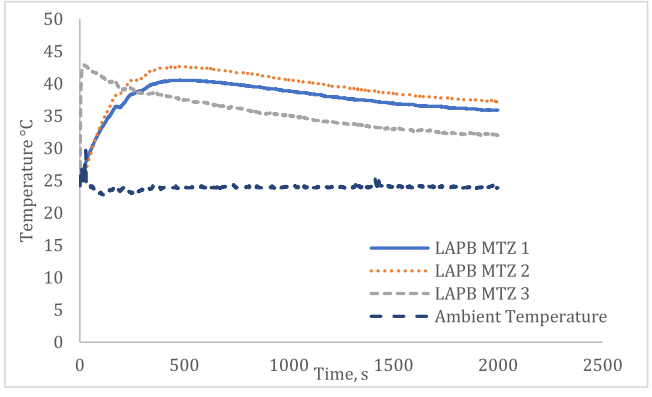

Fig. 12a. LAPB Temperature Distribution Across Bed

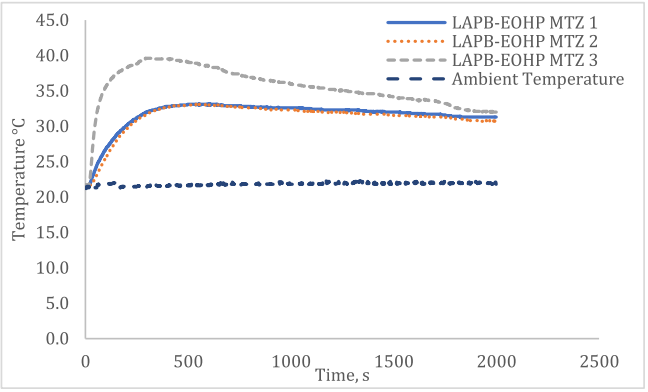

Fig. 12b. LAPB-EOHP Temperature Distribution Across Bed

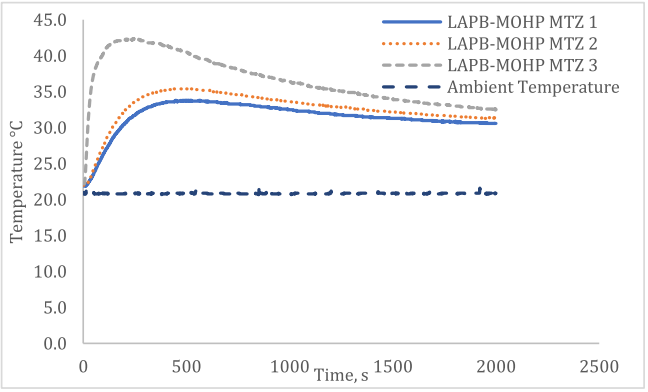

Fig. 12c. LAPB-MOHP Temperature Distribution Across Bed

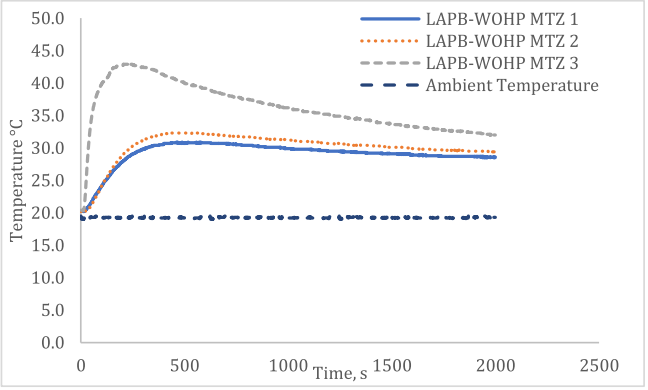

Fig. 12d. LAPB-WOHP Temperature Distribution Across Bed

while Table 9c shows the average bed and peak adsorption temperature values for the various mass transfer zones. As with these annulus configurations, the temperature rise initially begins in the MTZ 3 followed by the MTZ 2 and subsequently the MTZ 1. Here, it is observed that the peak adsorption and average bed temperatures in the mass transfer zones were higher in the MAPB packed bed than in its integrated MAPB-HCOHP systems. The variation in the performance of the HCOHPs was marked here. The WOHP appeared to significantly reduce the average and peak temperature values in the mass transfer zones followed by the MOHP and the EOHP. It is important to note that with the comparatively reduced fluid–solid mixing here compared to the LAPB configuration, equilibrium times for this configuration was comparatively longer. As can be seen in Fig. 13a, it also took a comparatively longer time to reach peak adsorption temperatures in MTZ 3 hence the ascent to peak here

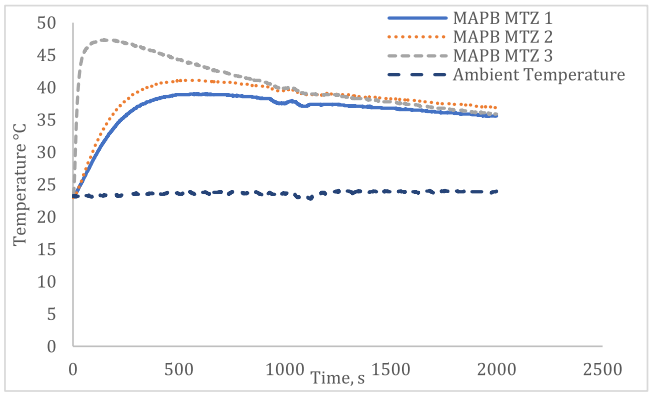

Fig. 13a. MAPB Temperature Distribution Across Bed

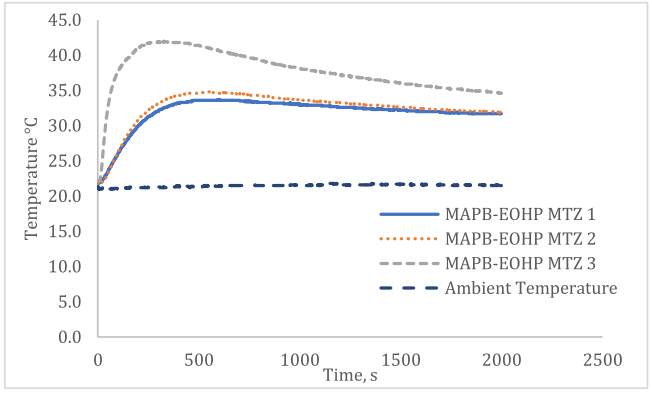

Fig. 13b. MAPB-EOHP Temperature Distribution Across Bed

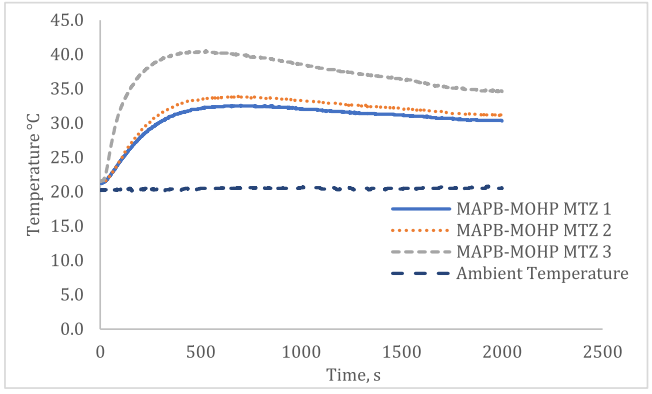

Fig. 13c. MAPB-MOHP Temperature Distribution Across Bed

was not as sharp as in the LAPB systems. For this MAPB system on its own, comparatively higher peak temperatures in the MTZ 3 were recorded due to the mass of silica gel available for adsorption. Here peak adsorption temperature reduction ranging between 5.4 °C and 10 °C were achieved in the MTZ 3 when the MAPB was integrated with the HCOHPs.

The Small Annulus Packed Bed (SAPB) has the smallest (D_o/D_i) and the largest mass of silica gel packing for the annulus packed beds as can be seen in Tables 3 and 4. The packed beds were randomly packed and the annulus dimension provided radial airflow for effective fluid–solid contact. From Fig. 14a and Table 9d, the SAPB with its relatively large silica gel mass recorded the maximum peak adsorption temperature in its MTZ 3 compared to the MAPB and LAPB systems. Here, there was a relatively longer lag in reaching the peak adsorption temperature

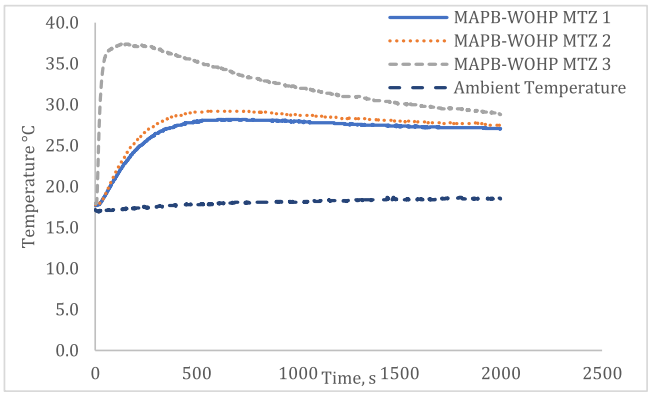

Fig. 13d. MAPB-WOHP Temperature Distribution Across Bed

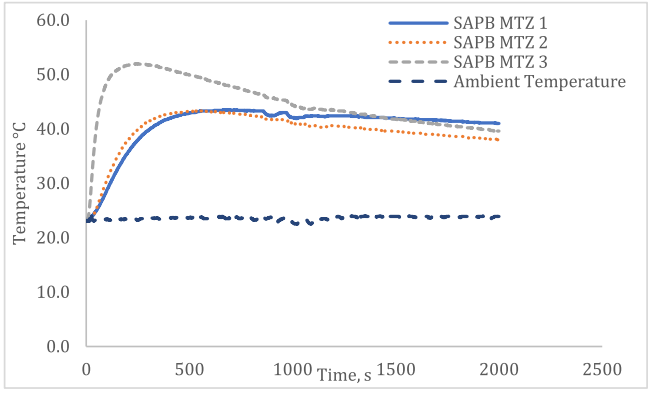

Fig. 14a. SAPB Temperature Distribution Across Bed

compared to the MAPB and the LAPB in that order. This configuration released more heat than the other two annular packed bed configurations due to its comparatively larger mass of silica gel for adsorption. As shown in Figs. 14a–d and Table 9d, the peak adsorption and average bed temperatures in the various mass transfer zones of the SAPB system decreased significantly on integration with the HCOHPs. It does also show that the HCOHPs performed well when the amount of heat released from the packed beds was relatively larger. Here peak adsorption temperature reductions ranged between 10.1 °C and 13.2 °C in the MTZ 3 when the SAPB was integrated with the HCOHPs.

In Table 9d, the MOHP appeared to have reduced the peak adsorption and average bed temperatures in MTZ 3 more than the other HCOHPs although in the other mass transfer zones the WOHP appears to perform better. This phenomenon appears to be linked with the start-up

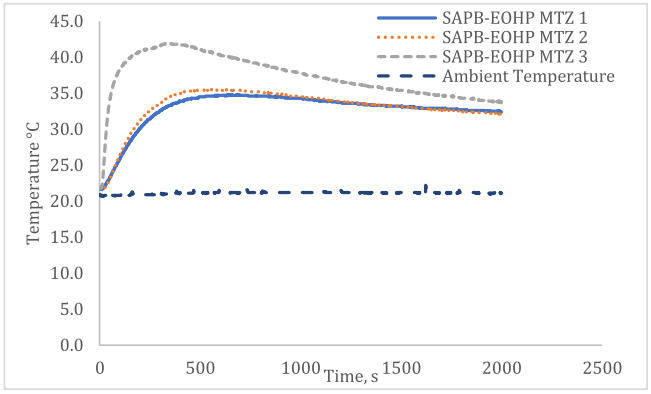

Fig. 14b. SAPB-EOHP Temperature Distribution Across Bed

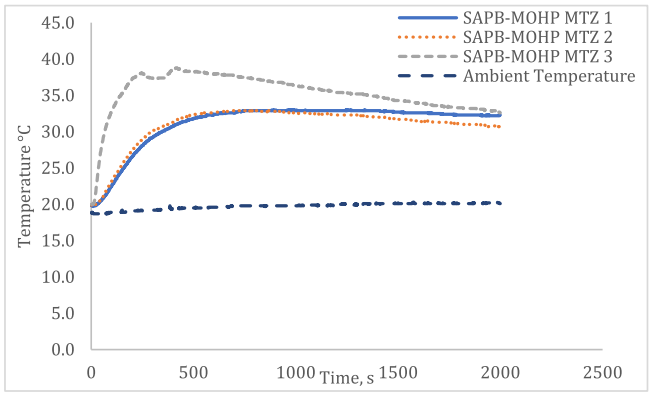

Fig. 14c. SAPB-MOHP Temperature Distribution Across Bed

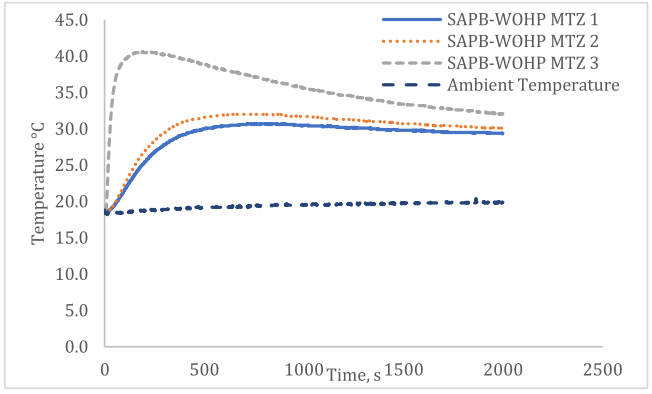

Fig. 14d. SAPB-WOHP Temperature Distribution Across Bed

behaviour of the HCOHPs in this case the MOHP started rejecting heat before the WOHP which is logical as it also has a lower boiling point under that evacuation pressure. The performance of the EOHP in this case was below that of the MOHP and WOHP. Overall, the HCOHPs were able to reduce the peak and average temperature values in the various mass transfer zones towards isothermal adsorption.

Generally, integrating the fully packed bed and its varied Heggs et al. [34] Z-annulus configurations with the HCOHPs reduced the average bed temperature significantly during adsorption. The reduction in temperature varied with the bed temperature of the unintegrated packed bed systems and the working fluid in the HCOHP. Here the HCOHPs thermal performance was instrumental in how much temperature reduction was attained. Peak adsorption temperatures in the mass transfer zones on the other hand varied mainly due to different start-ups of the HCOHPs.

3.3.2. *Outlet temperature*

Figs. 15a–d show the outlet temperatures differences for the packed beds and their corresponding integrated HCOHP systems. In Fig. 15a, averages of 8.3 °C, 7.0 °C and 7.5 °C were obtained respectively for the outlet temperature differences of the FPB and its integrated FPB-EOHP, FPB-MOHP and FPB-WOHP. For the LAPB and its integrated systems in Fig. 15b, averages of the outlet temperature differences were respectively 6.4 °C, 4.2 °C and 6.6 °C when integrated with the EOHP, MOHP and WOHP. At the peak of adsorption, the differences in outlet temperatures were far greater. The WOHP was observed to have reduce the outlet temperature of this packed bed configuration suddenly as the peak of adsorption was attained. The EOHP on the other hand gradually reduced the outlet temperature of this packed bed configuration. In Fig. 15c, average temperatures of 4.7 °C, 5.3 °C and 9.2 °C were recorded for the outlet temperature differences between the MAPB when

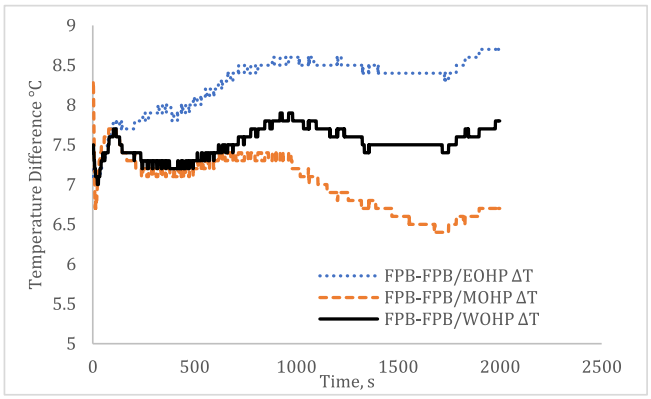

Fig. 15a. FPB and FPB-HCOHP Outlet Temperature Difference

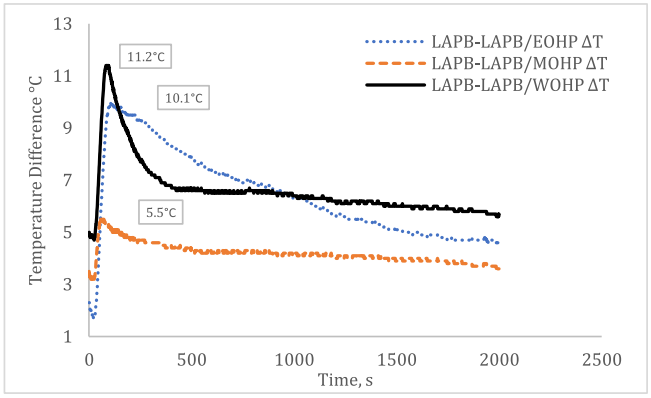

Fig. 15b. LAPB and LAPB-HCOHP Outlet Temperature Difference

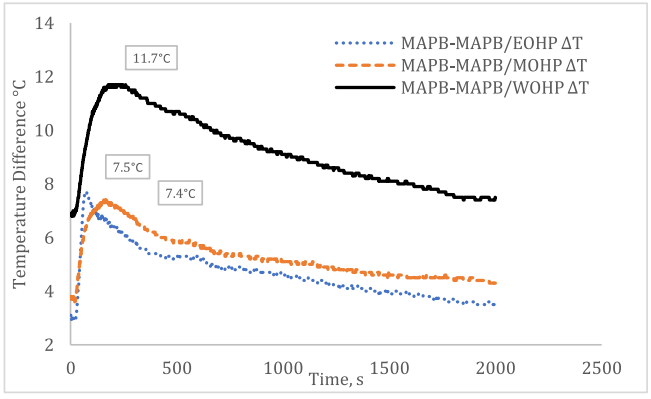

Fig. 15c. MAPB and MAPB-HCOHP Outlet Temperature Difference

integrated with the EOHP, MOHP and WOHP, respectively. In Fig. 15d, the SAPB and its integrated HCOHP systems had averages of the outlet temperature differences to be 4.2 °C, 6.6 °C and 6.3 °C when integrated with the EOHP, MOHP and WOHP, respectively. The performance of the MOHP and WOHP were comparable here while the EOHP was observed to have a lower reduction. Overall, integrating the various packed bed configurations with the HCOHPs reduced the outlet bed temperatures by varying amounts. The importance of the reduction in outlet temperature is that it has the potential to reduce the sensible cooling load hence having an overall influence on the energy efficiency of the solid desiccant cooling system.

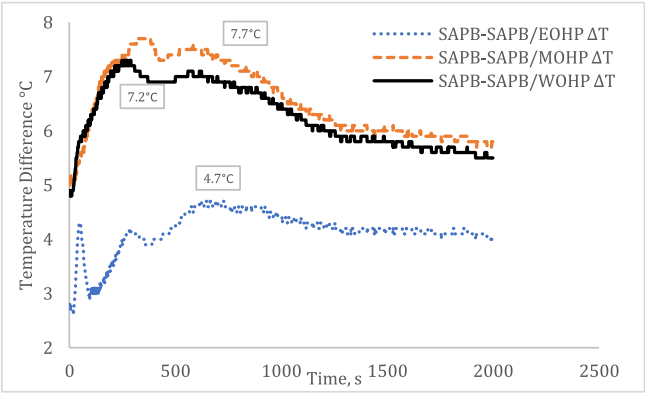

Fig. 15d. SAPB and SAPB-HCOHP Outlet Temperature Difference

3.4. Physical adsorption performance

3.4.1. The adsorption characteristics of the silica gel particles

The rate of water vapour adsorption is critical to the heat transfer process during solid desiccant–water vapour interactions. It is directly proportional to the specific surface area of solid desiccant particles and the difference between the vapour pressure in the gaseous phase and the vapour pressure at the surface of the particles [8]. The linear isotherm plot of the nitrogen adsorptive on the silica gel (SiO_2) is shown in Fig. 16. The plot was generated from the BET surface area analysis carried out using the Micromeritics ASAP 2020, Surface Area and Porosity Analyser. From the plot it shows that between relative pressures of 0.4 and 0.6 there is a hysteresis loop when more than 200 cm^3/g of the N_2 gas was adsorbed. The hysteresis loop observed for this silicon dioxide is characteristic of the type IV physisorption isotherm as presented in IUPAC [42]. According to IUPAC [42] the occurrence of the hysteresis loop is associated with capillary condensation taking place in mesopores, and the limiting uptake over a range of high p/p°. Since the isotherm did not exhibit low pressure ($\frac{p}{p^o} < 0.4$) with the adsorptive used in this case N_2, it can be concluded with relative certainty that there is some degree of accuracy with the results as stipulated by IUPAC [42]. The capillary condensation associated with the hysteresis loop observed in Fig. 16 represents multilayer adsorption from the water vapour where the pore spaces are filled with liquid separated from the gas phase by menisci [6].

3.4.2. Influence of the HCOHPs on adsorption performance

The outlet moisture content was determine from Eq. (4) using the outlet relative humidity obtained from the AZ8829 data logger. The mass flow rate was determined by the inlet moist air density from Table 1, the cross-sectional area in Table 5 and the outlet velocity of the air measured using the Sentry ST732 Hotwire Anemometer.

The rate of adsorption in the packed beds [1] using Eq. (9)

$$\dot{m}_{ads} = A \cdot u_o \cdot \rho(\omega_{in} - \omega_{out}) \quad (9)$$

In Fig. 17a, the adsorption rate in the FPB and its corresponding integrated HCOHP systems are presented. The adsorption rate for the FPB and its integrated FPB-EOHP, FPB-MOHP and FPB-WOHP respectively averaged 1.42×10^{-06}kg/s, 1.47×10^{-06}kg/s, 1.46×10^{-06}kg/s and 1.44×10^{-06}kg/s. It is important to note that unlike the Z-annulus variations of the packed bed, the fully packed structure of the FPB did not enhance airflow distribution within it due to the random full packing impeding the airflow distribution as observed by Yeboah and Darkwa [33]. From the average values, the integrated FPB-HCOHP systems showed a slightly improved adsorption capacity. It is also important to note that for this selected data, the FPB and its varied integrated HCOHP systems did not reach saturation.

Figs. 17b–d shows the adsorption rates for the annulus packed beds and their corresponding integrated HCOHP systems. It would be recalled that the annulus section provided radial flow of air through the beds and increased the fluid–solid contact. In Fig. 17b, the adsorption rate in the LAPB and its corresponding integrated HCOHP systems sharply declined over time. This packed bed system had least amount of silica gel for adsorption and the largest annulus dimension. For this reason, fluid solid mixing was comparatively vigorous here when a relatively large airflow was impeded by the end plate of the annulus section. As observed with the temperature profiles, this led to a quick ascent to the peak of adsorption before a quick decline as it approached saturation. The adsorption rate is observed to take a similar pattern here. It initially increases to a maximum before a sharp decline. The reason for the peak temperatures in the annulus packed beds corresponding with peak

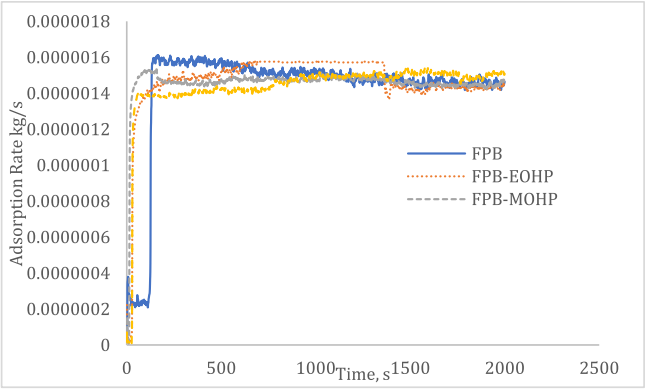

Fig. 17a. Adsorption Rate in the FPB and its Integrated HCOHP Systems

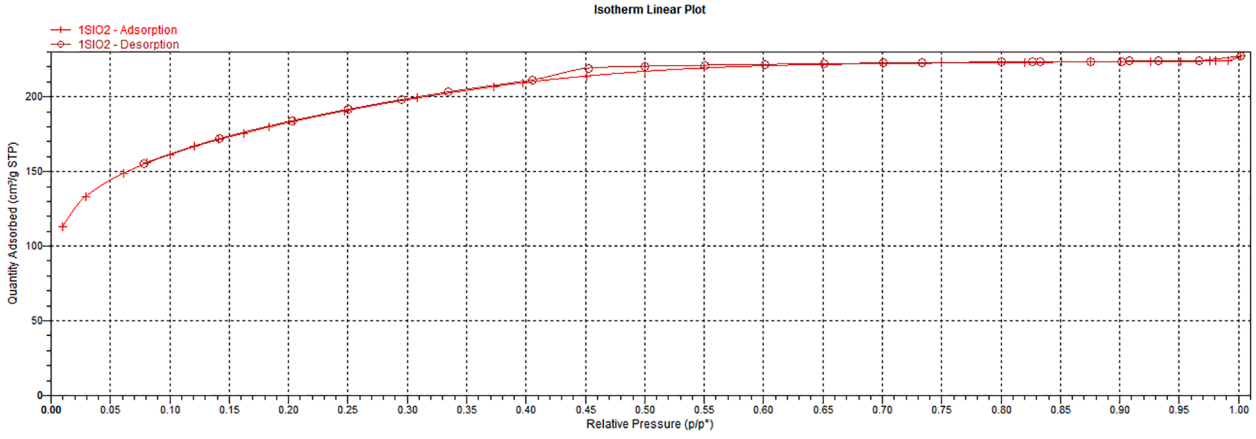

Fig. 16. Linear Isotherm Plot for the Silica Gel (SiO_2) Particles used in the Investigations

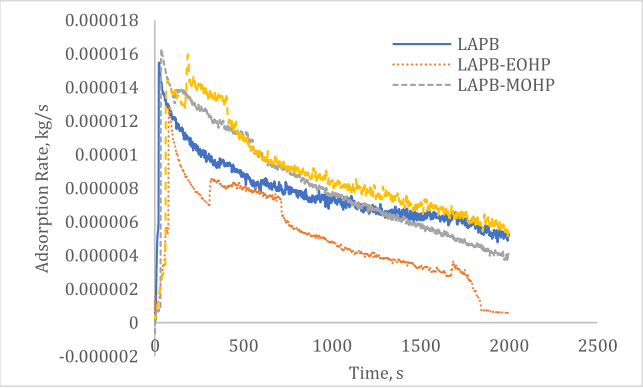

Fig. 17b. Adsorption Rate in the LAPB and its Integrated HCOHP Systems

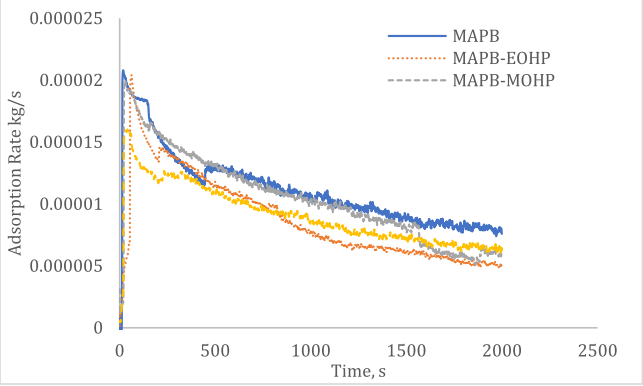

Fig. 17c. Adsorption Rate in the MAPB and its Integrated HCOHP Systems

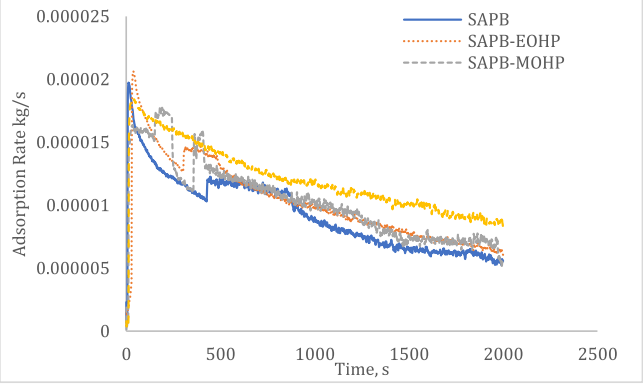

Fig. 17d. Adsorption Rate in the SAPB and its Integrated HCOHP Systems

adsorption rates as shown in Figs. 17b–d was to do with the vigorous fluid solid mixing in MTZ 3 and not the temperature of the bed. Here the end plate that created turbulent mixing is in this zone hence saturation was quickly reached due to effective fluid solid contact. Yeboah and Darkwa [33] found that the annulus inserts enhanced the adsorption process in the beds. Table 10 shows the averages of the rate of adsorption in the packed beds and corresponding integration systems. For the LAPB, it is shown that the overall adsorption rate increased when integrated with the MOHP and WOHP. The MAPB on the other hand did not show adsorption rate improvement on integration with the HCOHPs and adsorbed more moisture than the integrated MAPB-HCOHP systems (see Table 3). The rate of adsorption in the MAPB and its integrated HCOHP systems in Fig. 17c and Table 10 were inconsistent with the general trend observed for the LAPB and SAPB systems. For the SAPB, the

Table 10
Rate of moisture adsorption in the packed beds.

Packed Bed Configuration	Unintegrated (kg/s)	EOHP (kg/s)	MOHP (kg/s)	WOHP (kg/s)
FPB	1.42×10^{-06}	1.47×10^{-06}	1.46×10^{-06}	1.44×10^{-06}
LAPB	7.71×10^{-06}	5.04×10^{-06}	8.14×10^{-06}	8.81×10^{-06}
MAPB	1.11×10^{-05}	8.75×10^{-06}	1.04×10^{-05}	9.07×10^{-06}
SAPB	9.33×10^{-06}	1.03×10^{-05}	1.03×10^{-05}	1.21×10^{-05}

adsorption rates were higher when integrated with the HCOHPs. Although the rate of moisture adsorption in the packed beds and their integrated systems followed a similar declining trending for the annulus configurations, the total amount of moisture adsorbed (see Table 3) shows that on integration with the HCOHPs, the amount of moisture adsorbed increased. Here, the WOHP when integrated with the LAPB and SAPB performed very well. One key observation in Figs. 17b–d is that after 500 s, the rate of adsorption in the unintegrated packed beds starts improving. This time in Figs. 12–14 shows the period when the bed temperature was in sharp decline and the overall thermal resistance was increasing (see Figs. 7–9).

Largely, the rate of adsorption in the fully packed bed configurations were similar although the total amount of moisture adsorbed varied due to poor distribution of the moist air flow within them. For the annulus packed bed configurations, the rate of adsorption in MTZ 3 was largely influenced by the turbulent mixing due to the end plate of the annulus section impeding the air flow.

4. Uncertainty and error analysis

The absolute uncertainty values for the fundamental parameters are presented in Table 11. The values show the smallest division of the digital measurement devices used in obtaining the data. These values provide the range where the true measured value is likely to be, given that the equipment used in the experiments were calibrated properly.

The experimental results obtained for these integrated systems were contingent on several factors. It was observed that the inlet condition varied for all the individual unintegrated packed bed configurations and their respective integrated systems. This influenced moist air properties (see Table 1) that were used in determining the fluid phase contribution of the heat transfer within individual unintegrated packed beds and their respective integrated systems. Another situation where the results were likely to be impacted was with the slight variations in silica gel mass for the same configuration of individual unintegrated packed beds and their respective integrated systems.

Table 11
Absolute uncertainty values for fundamental parameters.

Parameter	Measurement Devices and Models	Absolute Uncertainty	Units
Pressure	QEALY Differential Pressure Meter	±0.001	Pa
Temperature	Omega K Type Thermocouples	±0.1	°C
Temperature	AZ 8829 sensor and data logger	±0.6 (from −20 ~ 50 °C), ±1.2 (others)	°C
Temperature	Sentry ST 732 Hotwire Anemometer	±2 (from −20 ~ 100 °C)	°C
Relative Humidity	AZ 8829 sensor and data logger	(Humidity Resolution ± 0.1) Accuracy ± 3	%
Velocity	Sentry ST 732 Hotwire Anemometer	±0.03 + 3%	m/s
Mass	HENGPING Scale Balance	±0.01	g

As established in Yeboah and Darkwa [33], the surrounding ambient condition potentially influenced the results obtained. This varied as the experiments were carried out several times over long periods spanning different seasons. Although the rig was insulated to ensure a relatively standard condition for the adsorption process, the ambient condition was difficult to control and impacted on the condition of the moist air supplied by the uninsulated uPvc mixing box.

In the charging of the HCOHPs with working fluid, the theoretical assumption was that the evacuated HCOHP devices maintained their evacuation pressure whilst being charged with working fluid. Although care was taken towards achieving that, its certainty is doubtful. The working fluid, deionized water manufactured from an in-house plant in the laboratory was assumed to be free of non-condensable gases and was not degassed before charging the HCOHPs. The ethanol and methanol were obtained from a commercial manufacturer who provided details of their properties. In the testing of the HCOHPs, they were fitted around the cylindrical copper vessel based on the assumption that all inner coil surfaces of the evaporator section were uniformly in contact with the outside walls of the cylindrical vessel. As presented in Yeboah and Darkwa [32] the evaluation of the HCOHPs showed there existed thermal contact resistance between it and the packed bed vessel. This resistance obviously influenced the heat transfer across the walls of the vessel to the evaporators of the HCOHPs.

The temperature data collected was sampled at the minimum 5.00 s interval for the setup in order to capture the oscillations in the measurement. However, earlier data collected with sample interval of 10.00 s presented no difference in the results demonstrating either the sensitivity of the thermocouples used or the Yokogawa MV2000′s capacity to capture the temperature signal within much smaller intervals.

5. Conclusions

Solid desiccant packed beds of varying configurations integrated with helically coiled oscillating heat pipes (HCOHPs) separately charged with ethanol, methanol and deionised water as working fluids, have been evaluated for their thermal effectiveness for isothermal adsorption. The results show that:

- Thermal contact resistance varied minimally for all the WOHP integrated systems ranging between 3.05×10^{-05} and 3.90×10^{-05}. For the EOHP integrated systems, the thermal contact resistance increased as heat input increased while for the MOHP a comparatively higher thermal contact resistance was recorded under all conditions. Here, the adsorption heat output profile did not seem to influence the transient thermal contact resistance of the integrated systems.
- Maximum peak adsorption temperature reductions of 20 °C was attained when the FPB was integrated with the HCOHPs while for the LAPB and its integrated systems a maximum of 3 °C peak adsorption temperature drop was achieved. For the MAPB and SAPB integrated systems, peak adsorption temperature reductions ranged between 5.4 °C and 10 °C and 10.1 °C to 13.2 °C, respectively.
- Average bed temperature reductions ranging between 12.6 °C and 14.0 °C, were achieved for the integrated FPB-HCOHP systems, 3.8 °C to 5.6 °C for the integrated LAPB-HCOHP systems, 4.4 °C to 9.5 °C for the integrated MAPB-HCOHP systems and 7.3 °C to 10.1 °C for the integrated SAPB-HCOHP systems. Maximum average bed temperature reduction of 14.0 °C between the FPB and the FPB-EOHP integrated system, 5.6 °C between the LAPB and the LAPB-WOHP integrated system, 9.5 °C between the MAPB and the MAPB-WOHP integrated system and 10.1 °C between the SAPB and the SAPB-WOHP integrated system were obtained.
- Adsorption rates were generally higher in the annulus packed bed configurations, largely influenced by turbulent mixing due to the end plate in MTZ 3 rather than thermal effects. For the random fully packed bed configuration there was mal-distribution of airflow resulting in reduced adsorption rates.

Overall, integrating the packed beds with the HCOHPs was found to remove the heat of adsorption released subsequently reducing the bed temperature. However, the HCOHPs performances in flattening the bed temperature was not only influenced by their overall thermal resistances but also their start-ups and the heat transfer resistance between their evaporators and the vessel walls. It is our view therefore that further optimization of the parameters of these integrated systems along with investigations of its regeneration potential be carried out for future practical applications.

CRediT authorship contribution statement

S.K. Yeboah: Conceptualization, Methodology, Validation, Formal analysis, Investigation, Writing - original draft, Visualization. **J. Darkwa:** Writing - review & editing, Supervision.

Declaration of Competing Interest

The authors declare that they have no known competing financial interests or personal relationships that could have appeared to influence the work reported in this paper.

References

[1] W.R. Abd-Elrahman, A.M. Hamed, S.H. El-Emam, M.M. Awad, Experimental investigation on the performance of radial flow desiccant bed using activated alumina, Appl. Therm. Eng. 31 (14-15) (2011) 2709–2715, https://doi.org/10.1016/j.applthermaleng.2011.04.041.
[2] K.A. Ramzy, R. Kadoli, T.P. Ashok Babu, Improved utilization of desiccant material in packed bed dehumidifier using composite particles, Renew. Energy 36 (2) (2011) 732–742, https://doi.org/10.1016/j.renene.2010.06.038.
[3] 9 ASHRAE Handbook - Fundamentals (SI Edition). American Society of Heating, Refrigerating and Air-Conditioning Engineers, Inc. ISBN 978-1-933742-55-7, pp 847–850.
[4] G.Q. Lu, X.S. Zhao, Nanoporous Materials - Science and Engineering. World Scientific Electronic ISBN 978-1-59124-984-9, 2004.
[5] P. Gandhidasan, A. Al-Farayedhi Abdulghani, Ali A. Al-Mubarak, Dehydration of natural gas using solid desiccants, Source Energy 26 (9) (2001) 855–868.
[6] IUPAC, Manual of symbols and terminology for physicochemical quantities and units- Appendix II. Pure & AppL Chem., Vol. 46, pp. 71—90. Pergamon Press, Printed in Great Britain, 1976.
[7] Mihajlo N. Golubovic, H.D.M. Hettiarachchi, William M. Worek, Sorption properties for different types of molecular sieve and their influence on optimum dehumidification performance of desiccant wheels, Int. J. Heat Mass Transf. 49 (17-18) (2006) 2802–2809, https://doi.org/10.1016/j.ijheatmasstransfer.2006.03.012.
[8] M.A. Rady, A.S. Huzayyin, E. Arquis, P. Monneyron, C. Lebot, E. Palomo, Study of heat and mass transfer in a dehumidifying desiccant bed with macro-encapsulated phase change materials, Renew. Energy 34 (3) (2009) 718–726, https://doi.org/10.1016/j.renene.2008.04.038.
[9] Ivan Pentchev, Kostadin Paev, Ilona Seikova, Dynamics of non-isothermal adsorption in packed bed of biporous zeolites, Chem. Eng. J. 85 (2–3) (2002) 245–257.
[10] Duong D. Do, Adsorption Analysis: Equilibria and Kinetics. Series on Chemical Engineering, Vol. 2. Imperial College Press, London, 1998.
[11] S.K. Yeboah, J. Darkwa, A critical review of thermal enhancement of packed beds for water vapour adsorption, Renew. Sustain. Energy Rev. 58 (2016) 1500–1520, https://doi.org/10.1016/j.rser.2015.12.134.
[12] C.E.L. Nobrega, N.C.L. Brum, Desiccant-Assisted Cooling: Fundamentals and Applications, Springer, London Heidelberg New York Dordrecht, 2014.
[13] Lorenzo Pistocchini, Silvia Garone, Mario Motta, Fluid dynamics optimization of a novel isothermal adsorption dehumidification system for solar driven applications, Energy Procedia 48 (2014) 628–637, https://doi.org/10.1016/j.egypro.2014.02.073.
[14] L. Meljac, V. Goetz, X. Py, Isothermal composite adsorbent. Part I: thermal characterisation, Source Appl. Therm. Eng. 27 (5–6) (2007) 1009–1016.
[15] Witold Kwapinski, Karijm Salem, Dieter Mewes, Evangelos Tsotsas, Thermal and flow effects during adsorption in conventional, diluted and annular packed beds, Chem. Eng. Sci. 65 (14) (2010) 4250–4260, https://doi.org/10.1016/j.ces.2010.04.017.
[16] Arthur L. Kohl, Richard B. Nielsen, Gas Purification, 5th ed., Elsevier, 1997. Electronic ISBN 978-0-0805-0720-0.
[17] M. Clausse, J. Bonjour, F. Meunier, Adsorption of gas mixtures in TSA adsorbers under various heat removal conditions, Chem. Eng. Sci. 59 (17) (2004) 3657–3670, https://doi.org/10.1016/j.ces.2004.05.027.

[18] Jocelyn Bonjour, Marc Clausse, Francis Meunier, A TSA process with indirect heating and cooling: parametric analysis and scaling-up to practical sizes, Chem. Eng. Process. Process Intensif. 44 (9) (2005) 969–977, https://doi.org/10.1016/j.cep.2005.01.002.
[19] Gerhard D. Pirngruber, F. Guillou, A. Gomez, M. Clausse, A theoretical analysis of the energy consumption of post-combustion CO2 capture processes by temperature swing adsorption using solid sorbents, Int. J. Greenhouse Gas Control 14 (2013) 74–83, https://doi.org/10.1016/j.ijggc.2013.01.010.
[20] Hamid Niazmand, Iman Dabzadeh, Numerical simulation of heat and mass transfer in adsorbent beds with annular fins, Int. J. Refrig. 35 (3) (2012) 581–593, https://doi.org/10.1016/j.ijrefrig.2011.05.013.
[21] Shivaji Sircar, Removal of heat of adsorption from adsorbent by forced convection, Adsorption 12 (3) (2006) 167–174, https://doi.org/10.1007/s10450-006-0143-2.
[22] B.N. Hung, A. Nuntaphan, T. Kiatsiriroat, Effect of internal cooling/heating coil on adsorption/regeneration of solid desiccant tray for controlling air humidity, Int. J. Energy Res. 32 (11) (2008) 980–987, https://doi.org/10.1002/er.1405.
[23] V.P. Mulgundmath, R.A. Jones, F.H. Tezel, J. Thibault, Fixed bed adsorption for the removal of carbon dioxide from nitrogen: breakthrough behaviour and modelling for heat and mass transfer, Sep. Purif. Technol. 85 (2012) 17–27, https://doi.org/10.1016/j.seppur.2011.07.038.
[24] Zirong Lin, Shuangfeng Wang, Jiepeng Huo, Yanxin Hu, Jinjian Chen, Winston Zhang, Eton Lee, Heat transfer characteristics and LED heat sink application of aluminum plate oscillating heat pipes, Appl. Therm. Eng. 31 (14-15) (2011) 2221–2229, https://doi.org/10.1016/j.applthermaleng.2011.03.003.
[25] N. Bhuwakietkumjohn, S. Rittidech, Internal flow patterns on heat transfer characteristics of a closed-loop oscillating heat-pipe with check valves using ethanol and a silver nano-ethanol mixture, Exp. Therm Fluid Sci. 34 (8) (2010) 1000–1007, https://doi.org/10.1016/j.expthermflusci.2010.03.003.
[26] H. Akachi, Structure of a Heat Pipe, U.S, Pat., 1990, p. 4921041.
[27] Jian Qu, Cheng Wang, Xiaojun Li, Hai Wang, Heat transfer performance of flexible oscillating heat pipes for electric/hybrid-electric vehicle battery thermal management, Appl. Therm. Eng. 135 (2018) 1–9, https://doi.org/10.1016/j.applthermaleng.2018.02.045.
[28] Aibo Wei, Jian Qu, Huihe Qiu, Cheng Wang, Gehan Cao, Heat transfer characteristics of plug-in oscillating heat pipe with binary-fluid mixtures for electric vehicle battery thermal management, Int. J. Heat Mass Transf. 135 (2019) 746–760, https://doi.org/10.1016/j.ijheatmasstransfer.2019.02.021.
[29] Jie Qu, Zhiqi Ke, Anhao Zuo, Zhonghao Rao, Experimental investigation on thermal performance of phase change material coupled with three-dimensional oscillating heat pipe (PCM/3D-OHP) for thermal management application, Int. J. Heat Mass Transf. 129 (2019) 773–782, https://doi.org/10.1016/j.ijheatmasstransfer.2018.10.019.
[30] Ning Qian, Xuesong Wang, Yucan Fu, Zhengcai Zhao, Jiuhua Xu, Jiajia Chen, Predicting heat transfer of oscillating heat pipes for machining processes based on extreme gradient boosting algorithm, Appl. Therm. Eng. 164 (2020) 114521, https://doi.org/10.1016/j.applthermaleng.2019.114521.
[31] Hai Wang, Jian Qu, Youquan Peng, Qin Sun, Heat transfer performance of a novel tubular oscillating heat pipe with sintered copper particles inside flat-plate evaporator and high-power LED heat sink application, Energy Convers. Manage. 189 (2019) 215–222, https://doi.org/10.1016/j.enconman.2019.03.093.
[32] S.K. Yeboah, J. Darkwa, Thermal performance of a novel helically coiled oscillating heat pipe (HCOHP) for isothermal adsorption. An experimental study, Int. J. Therm. Sci. 128 (2018) 49–58, https://doi.org/10.1016/j.ijthermalsci.2018.02.014.
[33] S.K. Yeboah, J. Darkwa, Experimental investigations into the adsorption enhancement in packed beds using Z-Annular flow configuration, Int. J. Therm. Sci. 136 (2019) 121–134, https://doi.org/10.1016/j.ijthermalsci.2018.10.027.
[34] Peter J. Heggs, David I. Ellis, Mohammed S. Ismail, The modelling of fluid-flow distributions in annular packed beds, Gas Separ. Purif. 8 (4) (1994) 257–264.
[35] Siegfried, Kwame, Yeboah, An integrated packed bed-oscillating heat pipe system for energy efficient isothermal adsorption processes, PhD thesis, University of Nottingham, 2017.
[36] Siegfried K. Yeboah, Jo Darkwa, Experimental Data on Helically Coiled Oscillating Heat Pipe (HCOHP) Design and Thermal Performance. Data in Brief In press, journal pre-proof. Available online 5 November 2020. Article 106505, 2020.
[37] M.M. Awad, K.A. Ramzy, A.M. Hamed, M.M. Bekheit, Theoretical and experimental investigation on the radial flow desiccant dehumidification bed, Appl. Therm. Eng. 28 (1) (2008) 75–85, https://doi.org/10.1016/j.applthermaleng.2006.12.018.
[38] Jian Qu, Huiying Wu, Ping Cheng, Start-up, heat transfer and flow characteristics of silicon-based micro pulsating heat pipes, Int. J. Heat Mass Transf. 55 (21-22) (2012) 6109–6120, https://doi.org/10.1016/j.ijheatmasstransfer.2012.06.024.
[39] CIBSE Guide C, Reference data, The Chartered Institution of Building Services Engineers London, 2007.
[40] A. Cengal Yunus, J. Ghajar Afshin, Heat and Mass Transfer: Fundamentals and Applications, Fourth Edition in SI Units. McGraw Hill, 2011, pp. 7–11.
[41] W.P. Jones, Air Conditioning Engineering, 5th ed., Butterworth Heinemann, 2005, pp 30–33.
[42] IUPAC, Reporting physisorption data for gas/solid systems: with special reference to the determination of surface area and porosity, Pure Appl. Chem. 57(4) (1984) 603–619. 1985, Printed in Great Britain.
[43] M. Thommes, Physical adsorption characterization of nanoporous materials, Chem. Ing. Tech. 82 (7) (2010) 1059–1073, https://doi.org/10.1002/cite.201000064.
[44] Hui T. Chua, Kim C. Ng, Anutosh Chakraborty, Nay M. Oo, Mohamed A. Othman, Adsorption characteristics of silica gel + water systems, J. Chem. Eng. Data 47 (5) (2002) 1177–1181, https://doi.org/10.1021/je0255067.
[45] L.S. Fletcher, D.A. Gyorog, Prediction of thermal contact conductance between similar metal surfaces in heat transfer and spacecraft thermal control, in: John W. Lucas (Ed.), American Institute of Aeronautics and Astronautics, 1971. ProQuest Ebook Central. http://ebookcentral.proquest.com/lib/unnc-ebooks/detail.action?docID=3111551. Created from unnc-ebooks on 2019-12-05 20:58:49.
[46] Ping Zhang, YiMin Xuan, Qiang Li, A high-precision instrumentation of measuring thermal contact resistance using reversible heat flux, Exp. Therm. Fluid Sci. 54 (2014) 204–211, https://doi.org/10.1016/j.expthermflusci.2013.12.012.
[47] J.P. Holman, Heat Transfer, 10th ed., McGraw-Hill, New York, 2010.
[48] Frank Kreith, Raj M. Manglik, Mark S. Bohn, Principles of Heat Transfer, 7th ed., CENGAGE Learning, 2011, p. A12.
[49] Tingting Hao, Xuehu Ma, Zhong Lan, Nan Li, Yuzhe Zhao, Hongbin Ma, Effects of hydrophilic surface on heat transfer performance and oscillating motion for an oscillating heat pipe, Int. J. Heat Mass Transf. 72 (2014) 50–65, https://doi.org/10.1016/j.ijheatmasstransfer.2014.01.007.
[50] Arno de Klerk, Voidage variation in packed beds at small column to particle diameter ratio, AIChE J. 49 (8) (2003) 2022–2029, https://doi.org/10.1002/aic.690490812.
[51] A.E. Kabeel, Adsorption–desorption operations of multilayer desiccant packed bed for dehumidification applications, Renew. Energy 34 (1) (2009) 255–265, https://doi.org/10.1016/j.renene.2008.04.011.